

# Damage-Tolerance Characteristics of Composite Fuselage Sandwich Structures With Thick Facesheets

David M. McGowan and Damodar R. Ambur  
Langley Research Center, Hampton, Virginia

February 1997

National Aeronautics and  
Space Administration  
Langley Research Center  
Hampton, Virginia 23681-0001

# **DAMAGE-TOLERANCE CHARACTERISTICS OF COMPOSITE FUSELAGE SANDWICH STRUCTURES WITH THICK FACESHEETS**

David M. McGowan and Damodar R. Ambur  
NASA Langley Research Center  
Hampton, VA 23681-0001

## **ABSTRACT**

Damage tolerance characteristics and results from experimental and analytical studies of a composite fuselage keel sandwich structure subjected to low-speed impact damage and discrete-source damage are presented. The test specimens are constructed from graphite-epoxy skins bonded to a honeycomb core, and they are representative of a highly loaded fuselage keel structure. Results of compression-after-impact (CAI) and notch-length sensitivity studies of 5-in.-wide by 10-in-long specimens are presented. A correlation between low-speed-impact dent depth, the associated damage area, and residual strength for different impact-energy levels is described; and a comparison of the strength for undamaged and damaged specimens with different notch-length-to-specimen-width ratios is presented. Surface strains in the facesheets of the undamaged specimens as well as surface strains that illustrate the load redistribution around the notch sites in the notched specimens are presented and compared with results from finite element analyses. Reductions in strength of as much as 53.1 percent for the impacted specimens and 64.7 percent for the notched specimens are observed.

## **INTRODUCTION**

One of the primary goals of the Advanced Composites Technology (ACT) program is to develop the enabling technology that will allow composite materials to be used in the primary wing and fuselage structures of the next generation advanced subsonic transport aircraft. As part of the ACT program, the Boeing Commercial Aircraft Group (BCAG) has been working to develop cost-effective and structurally efficient composite fuselage structure.<sup>1</sup> The focus of this work has been on the fuselage section just aft of the main landing gear wheel well of a modern wide-body transport which is designated as section 46 on a Boeing aircraft. This fuselage section is 33-feet long and 20-feet in diameter, and contains crown, side and keel quadrant sections as shown in Fig. 1.<sup>2</sup> As illustrated in Fig. 1, the current fuselage design concept utilizes skin-stringer construction in the crown quadrant section and sandwich construction in the side and keel quadrant sections.

Sandwich structures have been used extensively in stiffness-critical aircraft secondary structures. The application of sandwich structures in aircraft has been restricted in the past due to its undesirable moisture absorption and moisture retention characteristics, and due to an insufficient understanding of low-speed impact-damage mechanisms and the effect of such damage, as well as discrete-source damage, on the structural performance of such structures. Sandwich structures still have the potential for improved structural efficiency and reduced manufacturing cost. Now that sandwich concepts are being considered for application to aircraft primary structures, understanding the effects of low-speed impact damage and penetration damage on sandwich structures has become more important. A joint NASA/Boeing study has been conducted as part of the ACT program to address the technology issues associated with using composite-facesheet sandwich structure in subsonic transport fuselage side and keel panel applications. This study consisted of manufacturing, testing and analyzing full-scale keel- and side-quadrant-section sandwich panels.

As part of an ongoing effort to develop keel panel structure for section 46 of the fuselage, a keel panel representative of the forward part of the section 46 keel was designed and fabricated by the Boeing Commercial Airplane Group. The panel is constructed from graphite-epoxy facesheets varying in thickness along the panel length from 50 to 36 plies bonded to a fiberglass honeycomb core. An experimental and analytical study of this keel panel with thick facesheets was conducted at NASA Langley Research Center to understand the load distribution and failure mechanisms of the panel with and without impact and discrete-source damage.<sup>3</sup> The impact-damage conditions simulated in the experimental study of Ref. 3 correspond to barely visible impact damage (BVID). For the test panel studied, BVID was considered to have occurred when the residual dent depth on the facesheet measured at the impact site was greater than or equal to 0.05 in. or if the impact-energy level was equal to 100 ft-lb. The damage conditions at different locations of the panel corresponding to different impact-energy levels were determined using impact-damage screening-test results from another panel of the same design. The impact-damage screening-test results indicated that a significant amount of through-the-thickness damage occurred in the facesheet at much lower impact-energy levels than for monolithic laminates with the same construction features as the facesheets. Also, for impact-energy levels as high as 100 ft-lbs, the residual dent-depth values were much less than 0.05 in. for thick facesheet sandwich plates. These impact-damage characteristics also suggest that, for low-level impact-energy levels, considerable reduction in compression-after-impact strength occurs for the sandwich structures, and the reduction in strength could be much greater if a dent-depth value of 0.05 in. was used as a BVID criterion. The dent-depth criterion assumed in the study of Ref. 3 does not appear to be appropriate for the damage-tolerant design of sandwich structures with thick facesheets and needs further investigation.

Discrete-source damage was simulated in the study of Ref. 3 by machining a 2-in.-long notch across the specimen width through both facesheets of the panel. The ratio of the specimen width to the notch length for this specimen condition is equal to 5, which is adequate to avoid boundary effects on the panel response. There is currently a lack of information on the effect of notch size on the failure modes and residual strength of compression-loaded sandwich structures with thick facesheets that are candidates for aircraft primary structural applications.

The present paper describes the results of a compression-after-impact (CAI) study and a notch-length sensitivity study of specimens machined from the large fuselage test panel studied in Ref. 3. Experimental results for undamaged specimens will be compared with results from finite element analyses. The results of the CAI studies will provide a correlation between low-speed-impact dent depth, the associated damage area, and the residual strength for different impact-energy levels. A comparison of the undamaged and residual strength of specimens with different specimen-width-to-notch-length ratios will also be presented. Facesheet surface strains from the experiments that illustrate the load redistribution around the notch sites will be presented and compared with results from finite element analyses.

## **DESCRIPTION OF TEST SPECIMENS**

The forward keel panel test article studied in Ref. 3 is representative of the structure that would be used in the keel quadrant section of the highly compression loaded forward end of fuselage section 46. As discussed in Ref. 2, the current keel-quadrant-section design utilizes a solid 152-ply laminate at the forward end of section 46. As the magnitude of the compression loads become smaller towards the lightly loaded aft end of the keel quadrant section, the structure transitions to a sandwich construction with 12-ply facesheets at the aft end. To accommodate the changes in the thickness of the facesheets required to attain this transition, it is necessary that a certain number of plies be terminated or dropped in the facesheets along the length of the keel quadrant section. The fuselage forward keel panel studied in Ref. 3 is representative of this type of structure in that it has thick facesheets ( $\geq 36$ -ply laminates) and contains several dropped plies along the panel length.

The test panel studied in Ref. 3 was machined from a larger manufacturing demonstration panel that was fabricated to gain manufacturing scale-up experience with tow-placed composite structures with dropped plies.<sup>1</sup> This manufacturing demonstration panel, designated FK1, was designed and fabricated by the Boeing Commercial Airplane Group under NASA contract NAS1-18889 as part of

the ACT program. The facesheets are fabricated from Hercules, Inc. AS4/8552 graphite-epoxy pre-impregnated tow material using a tow placement manufacturing process. The honeycomb core is Hexcel, Corp. fiberglass Heat Resistant Phenolic (HRP) core material with a 3/16-in. cell size and a density of 12 lb/ft<sup>3</sup>. The core is co-bonded to the two facesheets using a film adhesive. Where plies are dropped in a facesheet, the outer thickness of the sandwich panel is maintained at a constant thickness by tapering the thickness of the core to match the inner surfaces of the facesheets. The details of the laminates used and the locations of the dropped plies in this panel are given in Ref. 3.

A total of twelve 5-in.-wide by 10-in.-long specimens were machined from the keel panel in Ref. 3 and the remnants of the larger manufacturing demonstration panel. These specimens have an outer mold line (OML) radius of curvature of 122 inches, and a constant thickness of 1.53 inches, as shown in Fig. 2. To obtain the number of specimens necessary for the present study (ten), some of the specimens were machined from areas of the panel that contain dropped plies. A total of eight different laminates appear in five of the ten specimens studied. The ply orientations for these laminates are given in Table I. A list of the specimen number, the type of test performed on each specimen, and the laminates contained in each specimen is given in Table II. As indicated in Table II, specimens 2 and 3 are identical to each other, while specimens 8, 9, and 10 are identical to each other. Schematic diagrams of these two sets of specimens that show the locations of these laminates in the different test specimens are given in Fig. 3. In Fig. 3, the dropped plies are represented by dashed lines, and the orientation of the dropped ply is shown near each line. The nominal elastic properties of the AS4/8552 pre-impregnated tow material are given in Table III.

## **APPARATUS AND TEST CONDITIONS**

Tests of ten 5-in.-wide by 10-in.-long specimens were conducted. These specimens were tested with three different damage conditions: undamaged, impact-damaged, and notched. The test matrix for the study is summarized in Table IV. The impact-energy levels selected for the compression-after-impact (CAI) tests were based on the results from the impact-damage screening tests presented in Ref. 3. Three notch lengths were selected to provide data for a range of specimen-width-to-notch-length ratios. The failure loads for all the specimens tested are summarized in Table IV.

The core at the five-inch-wide loaded ends of the specimens was removed to a depth of 0.5 inches, and epoxy resin material was potted between the facesheets to prevent an end-brooming failure. The potted ends were machined flat and parallel to each other to assure that a uniform load is applied to the specimen. The ten-inch-long edges were not supported. For the CAI tests, the OML surface of the

panel was painted white so that a shadow moiré interferometry technique could be used to monitor the out-of-plane displacements and to observe any local response such as delamination buckling and growth at the impact-damaged sites. For the notch-length sensitivity study, a photoelastic coating was applied to the OML so that surface strain gradients could be obtained using an optical photoelastic technique.<sup>4</sup> The details of the impact damage levels and the notches are described in the next section.

As indicated previously, a shadow moiré interferometry technique was used for the CAI tests to monitor out-of-plane displacements of the facesheets and to monitor damage growth around the damage sites. A 5-in.-wide by 9-in.-long area in the center of the panel was monitored on the convex surface of the panel. The moiré fringe patterns were recorded using still photography and video photography. The response of the concave surface of the panel was also recorded using video photography.

A 0.04-in.-thick PS-1 birefringent photoelastic coating made by the Measurements Group was used in this study. The photoelastic coating was bonded to the specimen with a premachined notch using PC-1 adhesive. After curing the adhesive, the notch geometry of the test specimen was machined into the photoelastic coating to match the test specimen. The response of the thick facesheet sandwich panels is not expected to be influenced by the photoelastic coating since the photoelastic coating has negligible inplane stiffness compared to the sandwich facesheet. The fringe coefficient of the photoelastic coating is 1875  $\mu\text{in./in.}$  per fringe order. A Vishay Model 031 reflection polariscope was used during the tests to obtain the color fringe information that represents the strain state in the specimen. The photoelastic fringe patterns were recorded using still photography, and the convex surface of the specimens were video taped to record the failure of the specimens.

For all tests, the potted ends of the specimens were loaded in uniaxial compression in a 300-kip-capacity hydraulic test machine. The test setup for the test of a notched specimen is shown in Fig. 4. The loaded edges of the specimens were clamped into a curved steel support fixture to provide a clamped boundary condition at those edges. The unloaded edges of the specimens were unsupported. Surface strains were measured using electrical resistance strain gages. Direct-current displacement transducers (DCDT's) were used to measure out-of-plane displacements of the facesheets as well as the stroke of the test machine loading platen. The locations of the strain gages for the undamaged specimens are shown in Fig. 5. The locations of the strain gages for the impacted and notched specimens are shown in Figs. 6 and 7, respectively. The axial load applied to the specimens was measured using the test machine load cell. The strain gage, DCDT, and load data were recorded using a digital data acquisition system. Data were taken at one second intervals while loading the specimens to failure.

## DESCRIPTION OF DAMAGE CONDITIONS

Both low-speed impact damage and discrete-source damage are simulated in the present study. A summary of the damage state in which each specimen was tested is presented in Table IV. The compression-after-impact (CAI) specimens were impacted using a dropped-weight impact apparatus<sup>5</sup> with an 11.8-lb mass and a 1-inch-diameter hemispherical tup. Impact energies ranging from 40 ft-lbs to 100 ft-lbs were used to impact the specimens. A schematic of the specimen support setup used to impact these specimens is shown in Fig. 8. As shown in the figure, the supports used consist of curved wooden supports and steel I-beams mounted to a rigid table. The specimens were clamped to the support beams to minimize specimen rebound after impact. Other specimen response parameters measured include the residual dent depth at the impact site and the area of the damaged site. The damage area was measured from the ultrasonic C-scan images of the damage site. The damage area in the CAI specimens is represented approximately by the circle of radius  $R$  in Fig. 6. The value of  $R$  for each specimen is indicated in the figure.

The impact energies used in the present study were selected based upon the results of the impact-damage screening tests described in Ref. 3. These screening tests showed that significant internal damage can occur for impact energies that are significantly lower than 100 ft-lbs even when the residual dent depth at the impact site is much smaller than 0.05 in. Measured values of the residual dent depth and damage area at the impact sites are summarized in Table V. As seen in the table, a dent depth value greater than or equal to 0.05 inches only occurred in specimen 4 that was impacted with an energy level of 100 ft-lbs. This specimen is constructed using the thinnest laminate in the structure (36 plies). The important trend to note in Table V is that a considerable amount of damage occurs for impact energies well below 100 ft-lbs. Furthermore, although the dent depth is only 0.013 inches for the thickest specimen (specimen 1) for an impact-energy level of 100 ft-lbs, the damaged area is 4.15 in<sup>2</sup>. Except for specimen 4, the impact-damage conditions simulated in the present study do not satisfy the conventional criteria for barely visible impact damage (BVID), and these conditions would be considered to be non-visible damage. The damaged sites on these specimens exhibited very little surface damage, and if this damage were to occur in-service on an aircraft structure, it is very likely that the damage would go undetected during a routine visual inspection. Therefore, for this less than BVID condition, the performance of the structure must not be degraded below the design strain value by this damage. The possibility that this type of impact damage might occur during the lifetime of a civil transport aircraft is not small. It is therefore important that the effect of this type of damage on the structural response of the fuselage structure be well understood and the appropriate BVID conditions

be defined. Results of studies of the effect of low-speed impact damage on the response of composite-facesheet sandwich structure is given in references 6-10.

Discrete-source damage is simulated in the present study by a notch machined through both facesheets at the mid-length of the specimen. The details of a typical notch are shown in Fig. 9. As shown in the figure, the length of the notch is 0.19 inches. Three specimens were tested with notch lengths varying from 1.0 to 2.0 inches. A summary of the notch lengths and different specimen-width-to-notch-length ratios is presented in Table VI. The facesheets for all three notched specimens are identical.

## **ANALYTICAL MODEL**

The undamaged and notched specimens were analyzed using the DIAL finite element code.<sup>11</sup> The specimens were modeled as a combination of several sandwich plates each having a different facesheet stacking sequence and sandwich core thickness. The dropped plies and variations in core thickness in the test panel were therefore accounted for. An eight-node modified thick-shell element was used for modeling the plate. These elements are shear deformable and account for the large shear deformations associated with sandwich construction. The finite element model of an undamaged specimen is shown in Fig. 10(a). This model has a total of 324 elements and a total of 5,080 active degrees of freedom. Load is applied to the model by specifying a uniform end shortening,  $\delta$ , at one of the five-inch-wide edges, as shown in the figure. The potted ends of the panel in the test fixture are not modeled; thus, the total length of the model is 9.0 inches. The effect of the potting is simulated by clamping the loaded edges of the model. The 10-inch-long unloaded edges of the model are free, and the wide-column buckling load is predicted to be 328 kips. The finite element model of a specimen with a 1-in.-long notch is shown in Fig. 10(b). This model has a total of 702 elements and a total of 10,941 active degrees of freedom. As shown in the figure, additional elements are used in the region of the notch to improve the mesh refinement to better represent the stress gradients in that region.

## **RESULTS AND DISCUSSION**

Experimental results are presented for the CAI and notch-length sensitivity studies, and analytical results are presented for the undamaged and notched specimens. Experimental load-shortening results and experimental and analytical global surface strain results are presented and compared for the



undamaged specimens. Experimental surface strain results around the impact sites are presented for the CAI tests. Experimental and analytical surface strain results around the notch sites are compared for the notch-length sensitivity studies. Finally, the failure modes for the specimens are described.

### **Compression-After-Impact (CAI) Study**

Load-shortening results are presented in Fig. 11(a) for specimens 1-3 and in Fig. 11(b) for specimens 4-7. As seen in Fig. 11(a), the global stiffness of specimens 1-3 is not affected by the presence of the impact damage. This trend is also noted for the thinner facesheet specimens 4-7. Impact damaged specimen 6 exhibited a higher stiffness than the others, which appears to be an anomaly. Experimental axial surface strain results are presented in Fig. 12(a) for specimens 1 - 3 and in Fig. 12(b) for specimens 4-7. The surface strain results presented in these figures are far field results near the loaded edge of the specimens. The strain values presented are averaged values of back-to-back strain gage pairs near the right and left edges of the specimens. As shown in Figs. 12, the far field strain values for all of the CAI specimens are very close to one another indicating that the impact damage has insignificant influence on the global axial stiffness of the specimens. Failure strains for specimens 1 and 4 with 100 ft-lbs of impact energy are approximately 5,000  $\mu\text{in./in.}$  suggesting that the current design practice of using 4,000-5,000  $\mu\text{in./in.}$  for the ultimate load condition is valid.

Experimental axial surface strain results for specimens 1 and 4 are given in Fig. 13(a) and 13(b), respectively. Load is presented in these figures as a function of strain at three locations around each of the impact sites. The strain data at location A are the same far field data presented in Fig. 12. Location B is very near the damage and is located on the axial centerline of the specimen. Location C is adjacent to the damage sites and is located on the horizontal centerline of each site. The strain data recorded for location B during the test of the undamaged specimen are also presented in each figure. The data in Fig. 13(a) indicate that the impact damage in the thicker specimens does not significantly affect the response of the structure in that region since the data for locations A and B are very similar (within 1 percent of each other). Furthermore, the data at location B for the undamaged-panel test are within 3 percent of the data for the impacted specimen at that location. At location C, the strain is approximately 22.5 percent greater than the strain at location A. These results indicate that the damage at this site does introduce a local stress concentration, but does not affect the stress state at a location that is slightly removed from the damage site. The data in Fig. 13(b) indicate that the impact damage in the thinner specimens does have an appreciable affect on the response of the panel in that region. The strains at location A are approximately 34.6 percent greater than the strains at location B. Furthermore,

the strains at location B for the undamaged specimen are 47.4 percent greater than those at location B for the impacted specimen. This difference in strains represents the effect of the impact damage on the response of the specimen since the data from location B for the undamaged specimen is close to that for location A for the impact-damaged specimen. The strains at location C are 2.38 times larger than those at location A at failure. Therefore, although the damaged area in specimen 4 is smaller than that in specimen 1, the stress concentration is much larger, and the load redistribution in the specimen is more extensive.

Normalized failure loads are shown as a function of residual dent depth, damaged area, and impact energy in Figs. 14, 15, and 16, respectively. In these figures, the failure loads for specimens 1 - 3 are normalized with respect to the failure load for the undamaged specimen 2. Similarly, the failure loads for specimens 4-7 are normalized with respect to the failure load for the undamaged specimen 7. As shown in Fig. 14, reductions in compression strength of approximately 50 percent result when the residual dent depth value is approximately 0.01 inches. This dent depth value is one-fifth of the threshold value for BVID. The maximum reduction in strength for the thicker specimens is 50.3 percent exhibited by specimen 1 with a residual dent depth of 0.013 inches. The maximum reduction in strength for the thinner specimens is 53.1 percent exhibited by specimen 6 with a residual dent depth of 0.0555 inches. The data in Figs. 15 and 16 exhibit similar trends and appear to be approaching an asymptotic value of the normalized failure load. The important result to note is that appreciable reductions in compression strength occurred in all of the CAI specimens even for conditions in which the impact damage would be considered to be non-visible. For the thinner facesheet sandwich specimens, the BVID criteria of 0.05-in. dent depth or 100 ft-lbs of impact energy appear to be valid. These BVID criteria need further evaluation for thicker facesheet sandwich structures.

Still photographs of the moiré fringe patterns at zero load and just prior to failure of specimen 6 are shown in Fig. 17. As shown in the figure, there was an appreciable amount of damage growth during the test. A typical failure mode is shown in Fig. 18. As shown in the figure, a compression failure occurred in the facesheet that was impact damaged. Following this failure, the sandwich specimen experienced significant bending, and the remaining facesheet failed in bending. The failure initiated in the impacted facesheet at the damage site. A trend noted during the tests is that only the impacted facesheet failed in the tests of specimens 1 and 4 (100 ft-lbs of impact energy). Both facesheets failed for all other specimens. This difference in failure mode is attributed to the fact that specimens 1 and 4 exhibited reductions in failure strength of greater than 50 percent when compared to the undamaged specimens. Therefore, the residual load in the specimen following failure of the damaged facesheet was not large enough to fail the second facesheet. The reductions in strength for the other specimens

were less than 50 percent, and the residual load in each of these specimens was large enough to fail the second facesheet also.

### **Notch-Length Sensitivity Study**

Finite element analysis results for specimen 10 without and with a 1.0-in.-long notch loaded by 79.2 kips of axial compression are presented in Figs. 19(a) and 19(b), respectively. The axial surface strain variations in the unnotched specimen are due to changes in specimen axial stiffness that is a result of terminated plies along the specimen length. The strain gradients in the notched specimen are severe at the edge of the notch and the applied load is redistributed around the notch. Maximum values of strain occur at a location that is very close to the notch tip in the width-direction of the specimen. The analytical surface strain results for specimen 10 with a 1-in.-long notch are compared with the experimental results for that specimen in Fig. 20. The experimental strain contours are those obtained using the optical photoelastic technique. Axial surface strains measured on the concave surface of the specimen are given in Fig. 20(b). The experimental and analytical strain magnitudes compare well with one another.

Load-shortening results are presented in Fig. 21 for notched specimens 8-10. As shown in the figure, there is a small effect of the notch length on the stiffness of the structure. Specimen 10, with the shortest notch, has the highest stiffness, while specimen 8, with the longest notch, has the lowest stiffness. Experimental axial surface strain results are presented in Fig. 22 for specimens 8-10. Once again, the surface strain results presented in these figures are far field results measured near the loaded edge of the specimens. The strain values are averaged values as described in the previous discussion of the CAI study. The effect of the notch length on the far field response of the structure is small. The strain values for specimens 9 and 10 are very close to each other, while the strain values for specimen 8 are higher than those for specimens 9 and 10 for a given load. Experimental axial surface strain results for specimens 10 and 8 are given in Figs. 23 (a) and (b), respectively. Load data are presented in this figure as a function of strain at three locations on the specimen. The strain data at location A are the same far field data presented in Figs. 21 and 22. Location B is very near the damage site and is located on the axial centerline of the specimens. Location C is at the notch tips and is located on the horizontal centerline of the specimen. The data in Fig. 23(a) indicate that the presence of the notch significantly affects the response of the structure in that region. The strain value at location A is approximately 4.02 times larger than that at location B for specimen 10. At location C, the strain value is approximately 2.22 times larger than the strain at location A. Similarly, the strain value at location A is approximately 6.07 times larger than that at location B for specimen 8. At location C, the strain value is approximately 3.17 times larger than the strain at location A. These results indicate that the

notch introduces a large local stress concentration, and it significantly affects the stress state slightly removed from the notch site.

Normalized failure loads are shown as a function of the notch length in Fig. 24 for specimens 8-10. In this figure, the failure loads for these specimens are normalized with respect to the failure load for the undamaged specimen 7. The trend shown in this figure is similar to that shown in Fig. 18 for the CAI specimens. However, the notched specimens exhibit a larger reduction in strength. Specimen 8, which has a 2.0-in-long notch, exhibits a 64.7 percent reduction in strength which corresponds to a normalized failure load of 0.353. The typical failure mode for these specimens is a compression failure of both facesheets that initiates at the notch. A photograph of the failure mode for specimen 10 is shown in Fig. 25.

## **CONCLUDING REMARKS**

The objectives of the present investigation are to study the damage tolerance characteristics of composite fuselage keel sandwich structure subjected to low-speed impact damage and discrete-source damage that is simulated by machining a notch through both facesheets. The fuselage keel structure is constructed of graphite-epoxy skins bonded to a honeycomb core, and is representative of a highly loaded fuselage keel structure. Compression-after-impact (CAI) and notch-length sensitivity studies of 5-in.-wide by 10-in-long specimens were performed. The load distribution in the facesheets of the specimens is studied using experimental and finite element analysis results. A correlation between low-speed-impact dent depth, the associated damage area, and residual strength for different impact-energy levels is described, and a comparison of the undamaged and residual strength of specimens with different notch-length-to-specimen-width ratios is presented.

Experimental results from the CAI study showed that a large reduction in strength can occur in thick-facesheet honeycomb sandwich structure even if the residual dent depth at the impact site is not very large. Results from ultrasonic C-scan inspections of the impacted specimens indicate that large areas of internal damage were caused by the impacts. This damage was also present in specimens for which the residual dent depth was less than 0.05 inches (the value selected to represent the threshold of barely visible impact damage (BVID)). Experimental surface strain results indicate that large stress concentrations were present at the impact sites, and that the presence of the impact damage affected the response of the structure in the regions slightly removed from the impact sites. Reductions in compression strength of up to 53.1 percent were caused by the impact damage. The residual dent depth in the specimen exhibiting this reduction is 0.0555 inches. The failure mode of these specimens

is a compression failure that initiates at the impact damage site of the impact-damaged facesheet and a bending failure of the undamaged facesheet and. From the results of this investigation, it appears that the 0.05-in. dent depth or 100 ft-lbs of impact energy BVID criteria are applicable only to sandwich structures with a certain thickness facesheet and different criteria are required for thick-facesheet sandwich structures.

Experimental results from the notch-length sensitivity study show that large reductions in compression strength occur for notched thick-facesheet honeycomb sandwich structure. Experimental surface strain results indicate that large stress concentrations were present at the notch sites, and that the presence of the notch affected the response of the structure in the regions slightly removed from the impact sites. Reductions in compression strength of up to 64.7 percent are noted. The failure mode of these specimens is a compression failure of both facesheets that initiates at the notch.

## REFERENCES

1. Smith, P. J.; Ilcewicz, L. B.; and Olson, J. T.: Advanced Technology Composite Fuselage. Proceedings of the Fifth NASA/DoD/ARPA Advanced Composites Technology Conference, NASA CP-3294, 1995, pp. 1-31.
2. Avery, W. B.; Flynn, B. W.; Hanson, C. T.; Scholz, D. B.; Murphy, D. P.; Carberry, D. J.; Dopker, B.; Williams, A. M.; and Ilcewicz, L. B.: Design and Structural Development of a Composite Fuselage Keel Panel. Proceedings of the Fifth NASA/DoD/ARPA Advanced Composites Technology Conference, NASA CP-3294, 1995, pp. 463-496.
3. McGowan, D. M.; and Ambur, D. R.: Compression Response of a Sandwich Fuselage Keel Panel With and Without Damage. Presented at the Sixth NASA/DoD/ARPA Advanced Composites Technology Conference, Anaheim, CA, August 7-11, 1995.
4. Dally, J. W.; and Riley, W. F.: *Experimental Stress Analysis, Third Edition.*, Chapters 12-13. McGraw-Hill, Inc., New York, NY, 1991.
5. Ambur, D. R.; Prasad, C. B.; and Waters, W. A.: An Internally Damped, Self-Arresting Dropped Weight Apparatus for Studying the Low-Speed Impact Response of Composite Structures. *Journal of Experimental Mechanics*, Vol. 33, No. 1, March 1995, pp. 64-69.

6. Ambur, D. R.; and Cruz, J. R.: Low-Speed Impact Response Characteristics of Composite Sandwich Plates. AIAA Paper 95-1460, April 1995.
7. Bernard, M. L.; and Lagace, P. A.: Impact Resistance of Composite Sandwich Plates. *Journal of Reinforced Plastics and Composites*, Vol. 8, September 1989, pp. 432-445.
8. Tsang, P. H. W.; and Dugundji, J.: Damage Resistance of Graphite-Epoxy Sandwich Panels Under Low Speed Impacts. *Journal of the American Helicopter Society*, Vol. 37, No. 1, January 1992, pp. 75-81.
9. Koller, M. G.: Elastic Impact of Spheres on Sandwich Plates. *Journal of Applied Mathematics and Physics*, Vol. 37, March 1986, pp. 256-269.
10. Lee, L. J.; Huang, K. Y.; and Fann, Y. J.: Dynamic Responses of Composite Sandwich Plates Impacted by a Rigid Ball. *Journal of Composite Materials*, Vol. 27, No. 13, 1993, pp. 1238-1256.
11. Anonymous: *DIAL Finite Element Structural Analysis System, Version L3D3*. Lockheed Missiles and Space Company, August, 1991.

Table I. Details of facesheet laminate ply stacking sequences.

Laminate 1 (50 plies) - Thickest laminate
$[\pm 45 / 0 / + 45 / 90 / 0 / - 45 / 0 / + 45 / 90 / 0 / - 45 / 90 / 0 / \pm 45 / 0 / - 45 / 90 / 0 / + 45 / 0 / \pm 45 / 0]_s$
Laminate 2 (48 plies)
$[\pm 45 / 0 / + 45 / 90 / 0 / - 45 / 0 / + 45 / 90 / 0 / - 45 / 90 / 0 / + 45 / 0 / - 45 / 90 / 0 / + 45 / 0 / \pm 45 / 0]_s$
Laminate 3 (46 plies)
$[\pm 45 / 0 / + 45 / 90 / 0 / - 45 / 0 / + 45 / 90 / 0 / - 45 / 90 / + 45 / 0 / - 45 / 90 / 0 / + 45 / 0 / \pm 45 / 0]_s$
Laminate 4 (43 plies)
$[\pm 45 / 0 / + 45 / 90 / 0 / - 45 / 0 / + 45 / 90 / 0 / - 45 / 90 / + 45 / 0 / - 45 / 90 / 0 / + 45 / 0 / + 45 / 0_2 / - 45 / 0 / + 45 / 0 / 90 / - 45 / 0 / + 45 / 90 / - 45 / 0 / + 45 / 0 / - 45 / 0 / 90 / + 45 / 0 / \mp 45]$
Laminate 5 (41 plies)
$[\pm 45 / 0 / + 45 / 90 / - 45 / 0 / + 45 / 90 / 0 / - 45 / 90 / + 45 / 0 / - 45 / 90 / 0 / + 45 / 0 / + 45 / 0_2 / - 45 / 0 / + 45 / 0 / 90 / - 45 / 0 / + 45 / 90 / - 45 / 0 / + 45 / 0 / - 45 / 90 / + 45 / 0 / \mp 45]$
Laminate 6 (40 plies)
$[\pm 45 / 0 / + 45 / 90 / - 45 / 0 / + 45 / 0 / - 45 / 90 / + 45 / 0 / - 45 / 90 / 0 / + 45 / 0 / + 45 / 0_2 / - 45 / 0 / + 45 / 0 / 90 / - 45 / 0 / + 45 / 90 / - 45 / 0 / + 45 / 0 / - 45 / 90 / + 45 / 0 / \mp 45]$
Laminate 7 (38 plies)
$[\pm 45 / 0 / + 45 / 90 / - 45 / 0_2 / - 45 / 90 / + 45 / 0 / - 45 / 90 / 0 / + 45 / 0 / + 45 / 0_2 / - 45 / 0 / + 45 / 0 / 90 / - 45 / 0 / + 45 / 90 / - 45 / 0_2 / - 45 / 90 / + 45 / 0 / \mp 45]$
Laminate 8 (36 plies) - Thinnest laminate
$[\pm 45 / 0 / + 45 / 90 / - 45 / 0_2 / (-45 / 90 / + 45 / 0)_2 / + 45 / 0_2 / (-45 / 0 / + 45 / 90)_2 / - 45 / 0_2 / - 45 / 90 / + 45 / 0 / \mp 45]$

Table II. Summary of tests performed and laminates used in each specimen.

Specimen number	Type of test	Laminates contained in specimen
1	CAI	1
2	Undamaged	1-3
3	CAI	1-3
4-6	CAI	8
7	Undamaged	8
8-10	Notch-length sensitivity	4-7

Table III. Nominal elastic properties of AS4/8552 graphite-epoxy pre-impregnated tow material.

$E_{11}$ , msi	$E_{22}$ , msi	$G_{12}$ , msi	$\nu_{12}$	Ply thickness, in
17.8	1.36	0.766	0.32	0.0073

Table IV. Summary of damage state and failure loads.

Specimen number	Damage state	Failure load, lbs.
1	100 ft-lbs impact	139,600
2	Undamaged	280,800
3	60 ft-lbs impact	173,500
4	100 ft-lbs impact	103,500
5	60 ft-lbs impact	120,000
6	40 ft-lbs impact	131,300
7	Undamaged	220,700
8	2.0-in notch	77,800
9	1.5-in notch	87,200
10	1.0-in notch	111,700

Table V. Summary of residual dent depth and damaged area at impact sites.

Specimen number	Impact energy, ft-lbs	Residual dent depth, in.	Damaged area, in <sup>2</sup>	Normalized failure load
1	100	0.0130	4.007	0.497 <sup>a</sup>
3	60	0.0085	1.899	0.618 <sup>a</sup>
4	100	0.0555	3.295	0.469 <sup>b</sup>
5	60	0.0110	2.475	0.544 <sup>b</sup>
6	40	0.0095	1.690	0.595 <sup>b</sup>

<sup>a</sup>normalized with respect to the failure load for specimen 2<sup>b</sup>normalized with respect to the failure load for specimen 7

Table VI. Summary of specimen-width-to-notch length ratios (w/d).

Specimen number	Notch length, d, in.	w/d	Normalized failure load <sup>a</sup>
8	2.0	2.5	0.352
9	1.5	3.3	0.395
10	1.0	5	0.506

<sup>a</sup>normalized with respect to the failure load for specimen 7



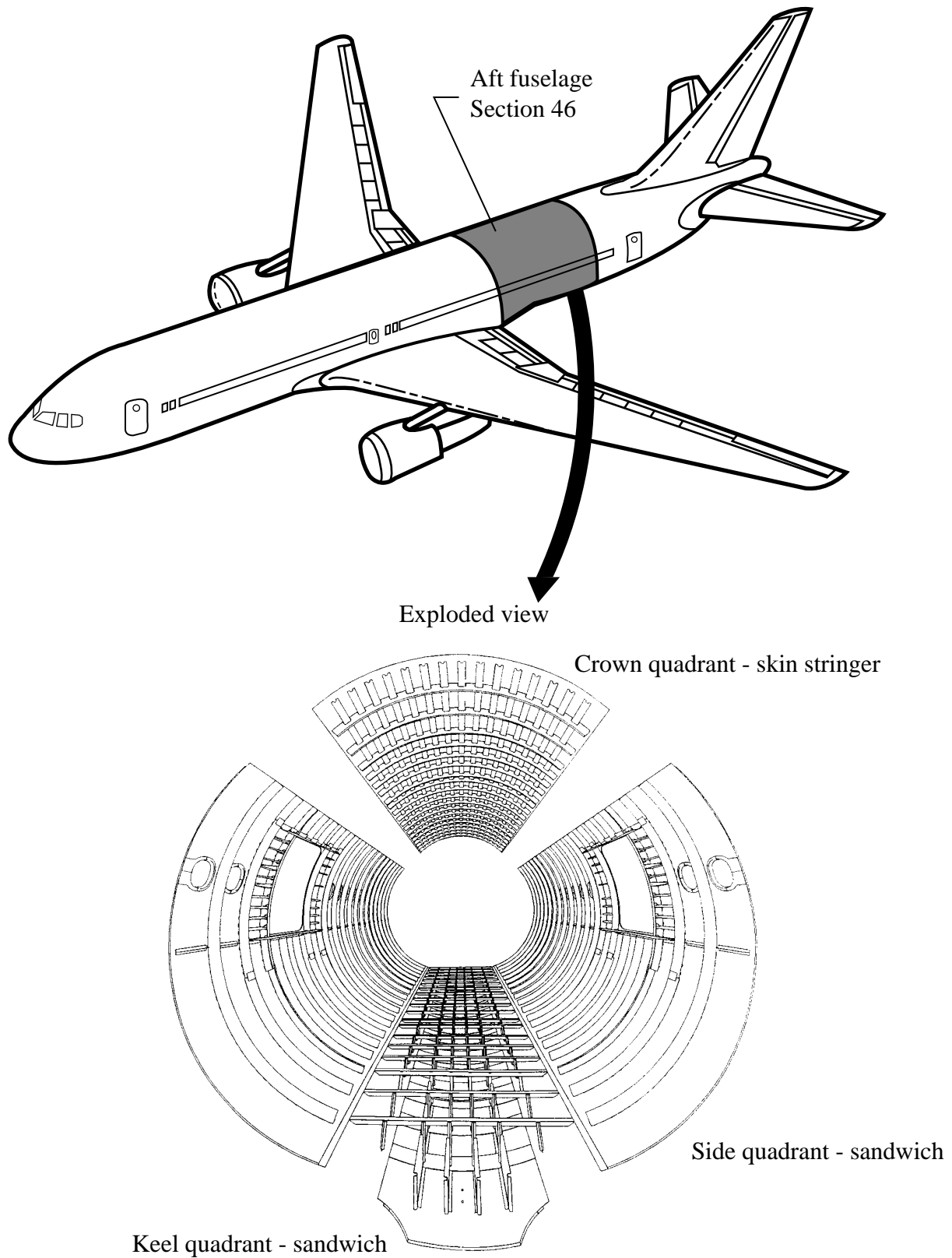


Figure 1. Details of a generic wide-body transport aircraft fuselage structure.

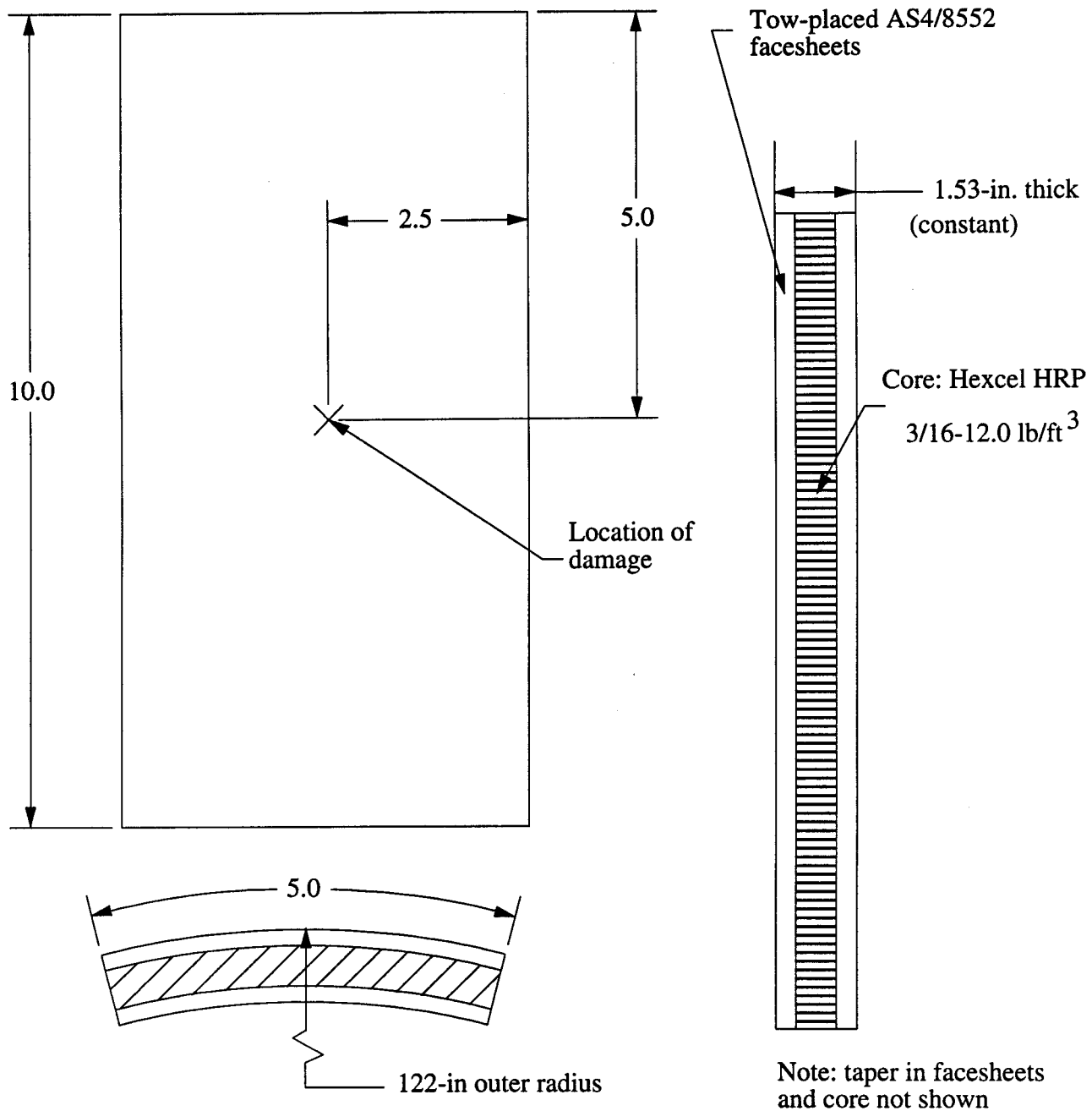


Figure 2. Geometry of test specimens. Dimensions are in inches.

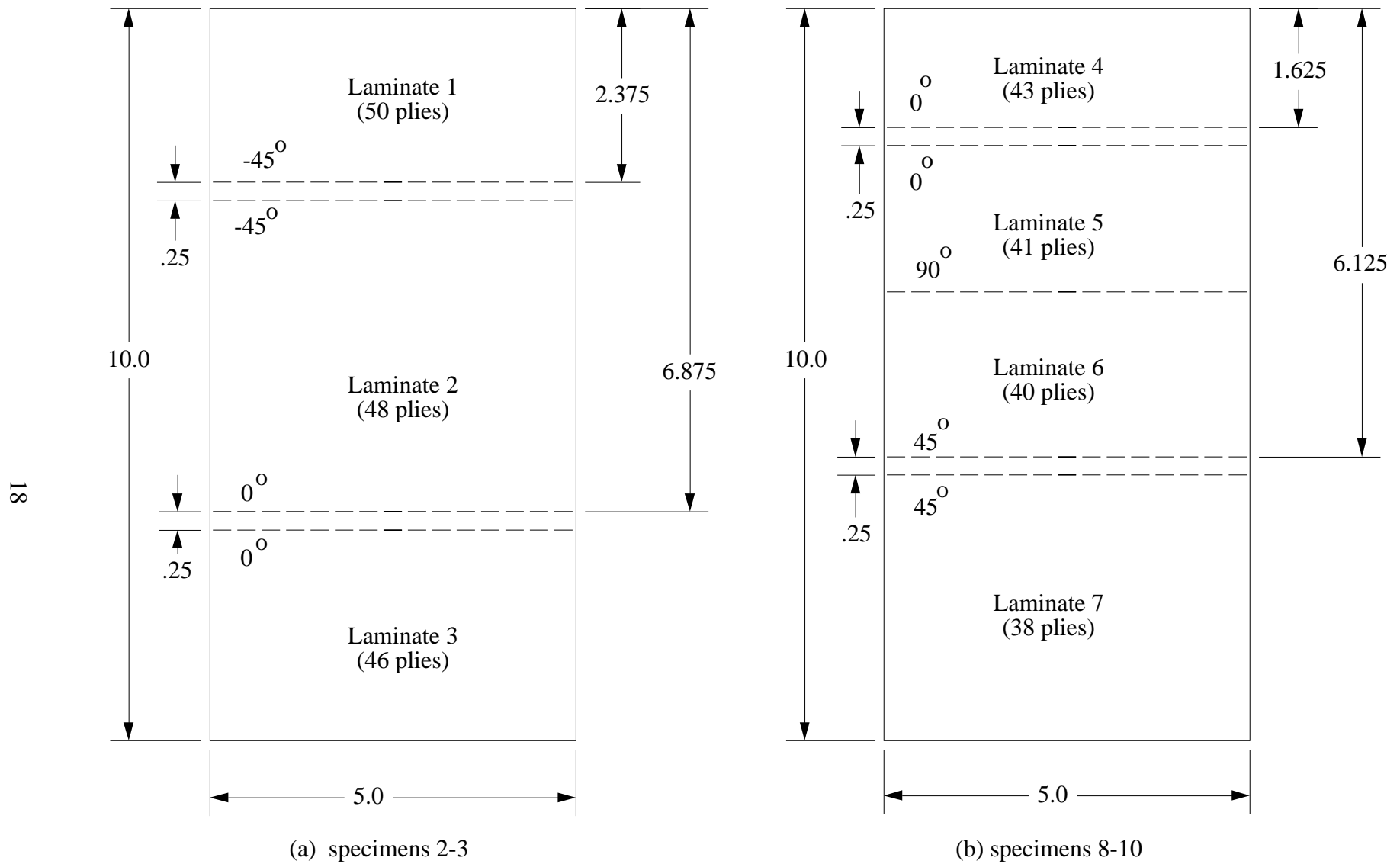


Figure 3. Locations of terminated plies in specimens 2, 3, 8, 9, and 10. Dimensions are in inches.

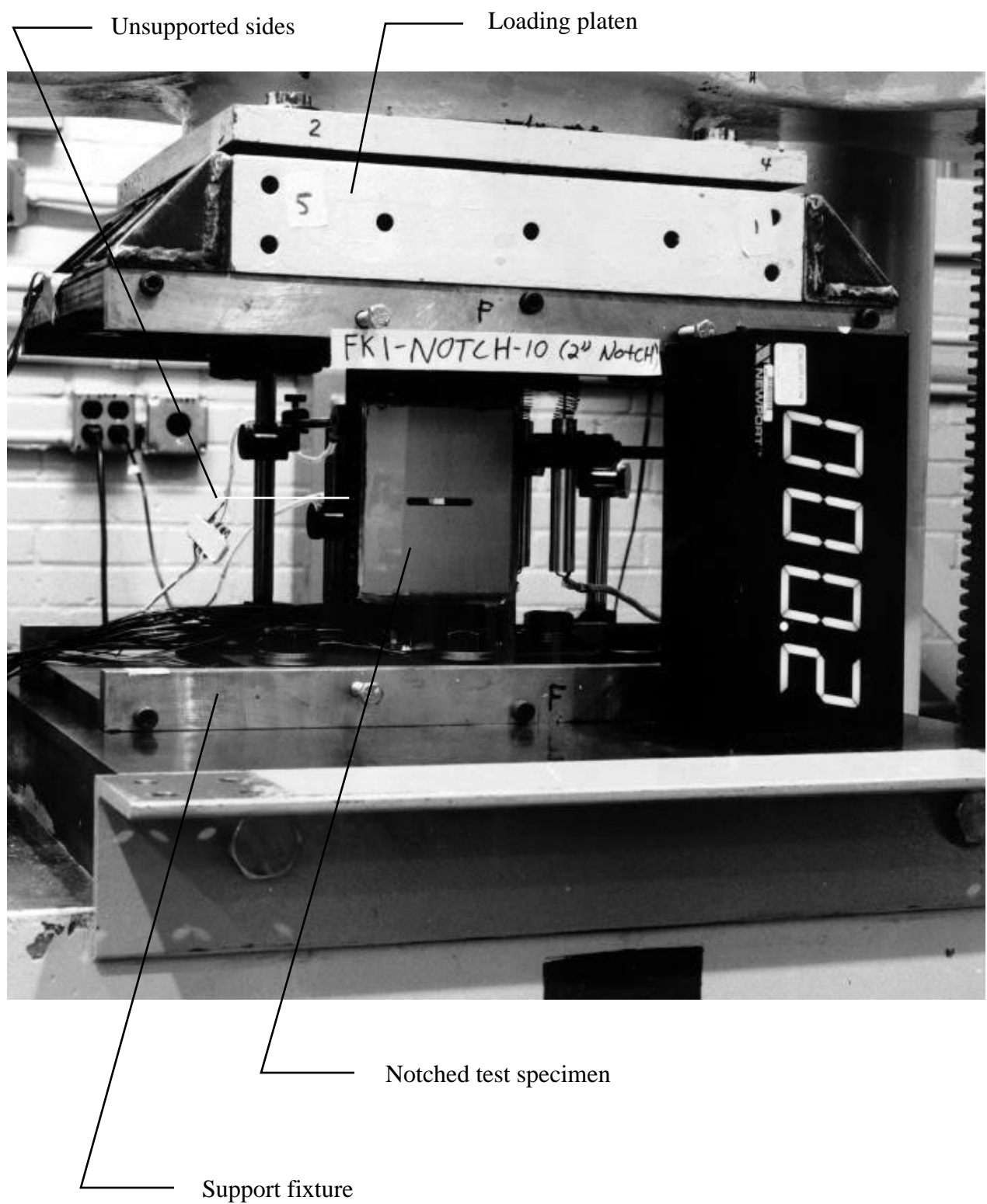


Figure 4. Typical axial compression test setup.

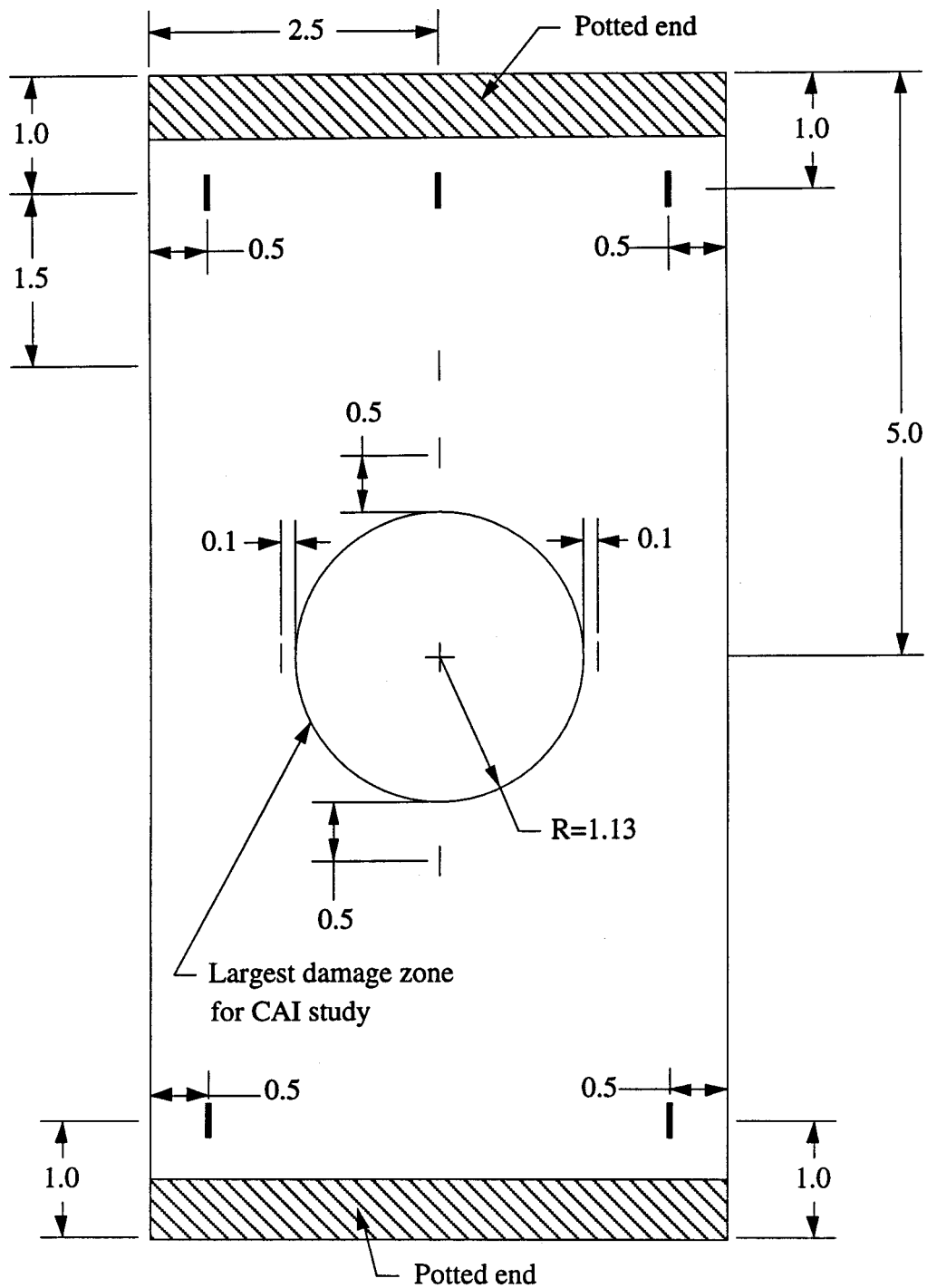


Figure 5. Strain gage layout for undamaged specimens 2 and 7. Dimensions are in inches. View from specimen convex surface. Bold lines indicate back-to-back strain gage pairs, all other gages are mounted on convex surface.

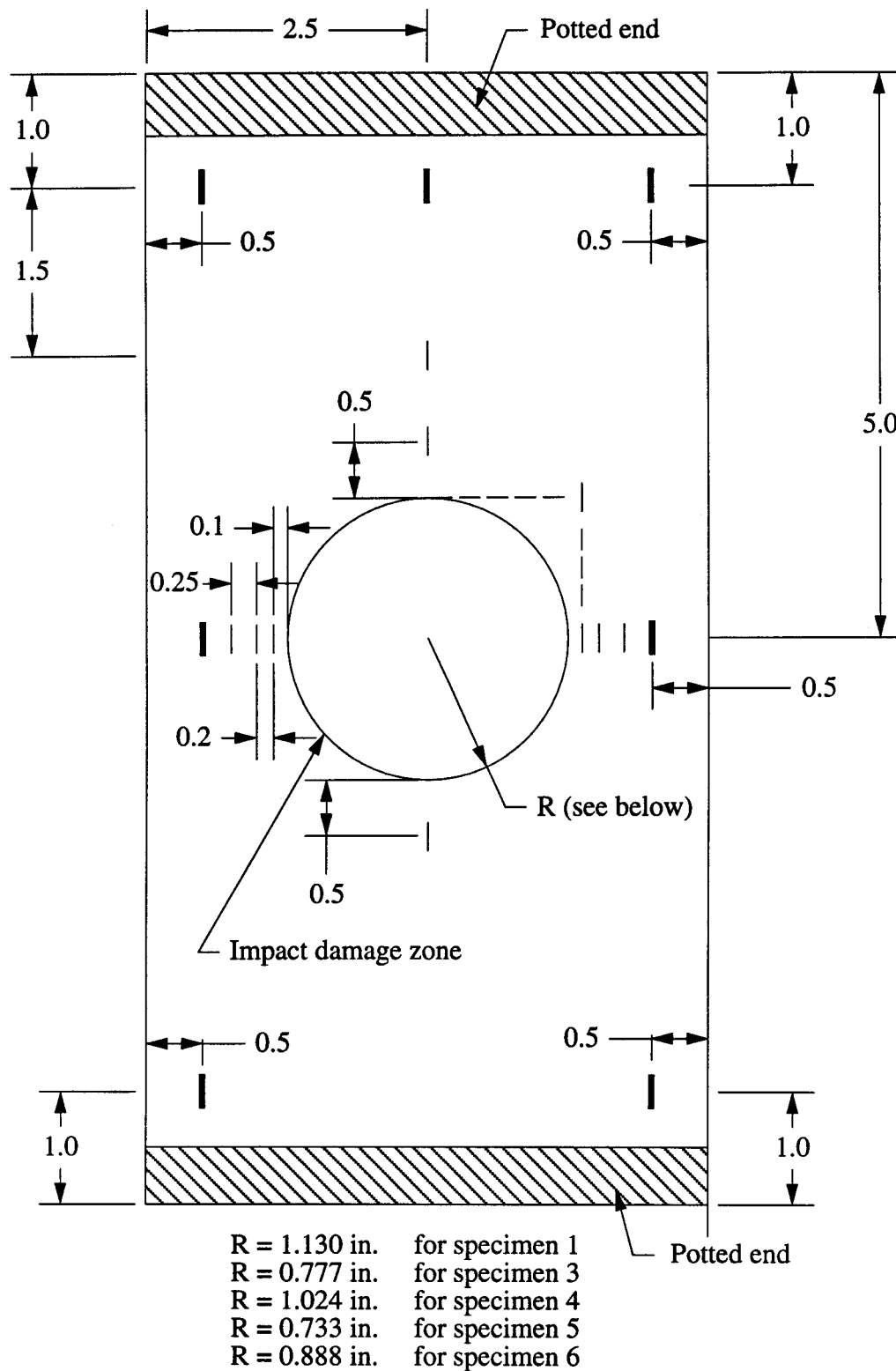


Figure 6. Strain gage layout for CAI specimens 1, 3, 4, 5, and 6. Dimensions are in inches. Viewed from the specimen convex surface. Bold lines indicate back-to-back strain gage pairs, all other gages are mounted on the specimen convex surface.

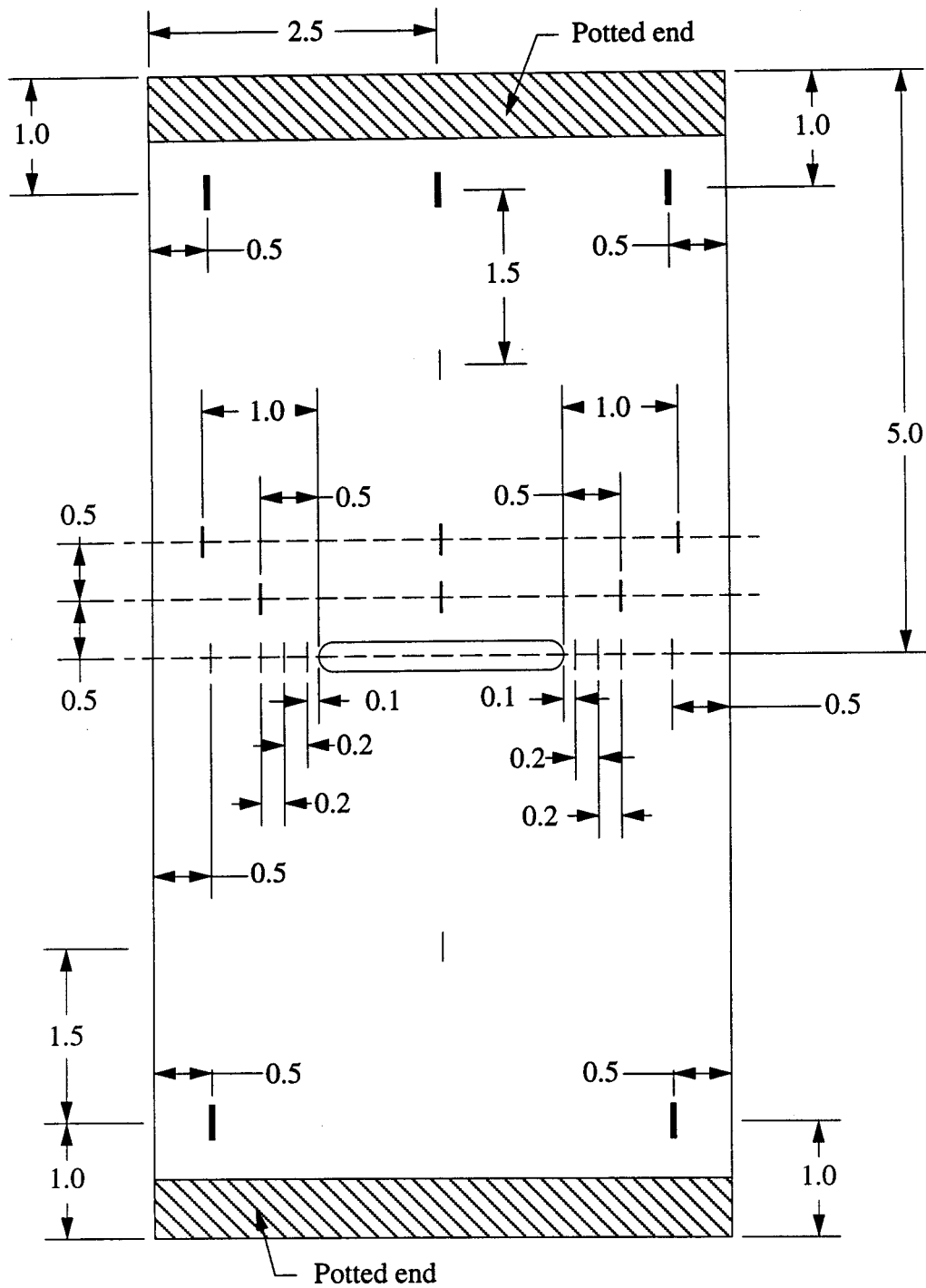
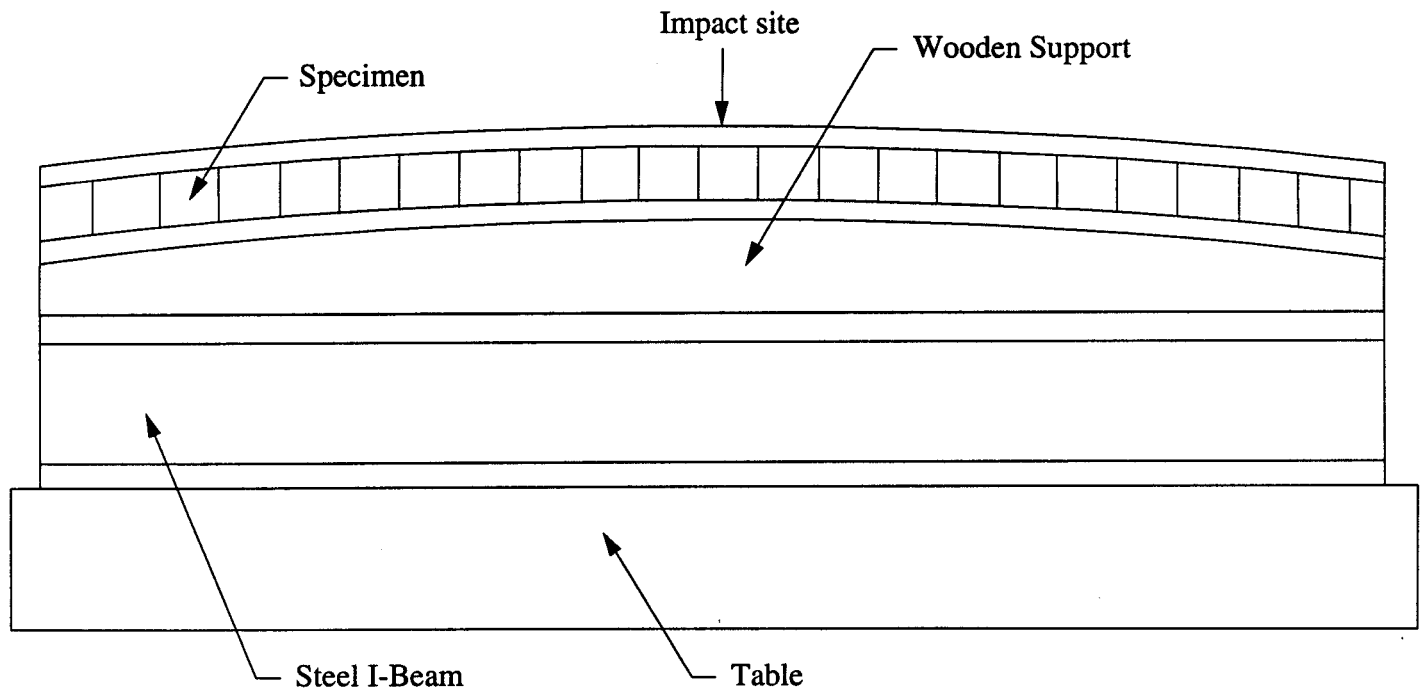
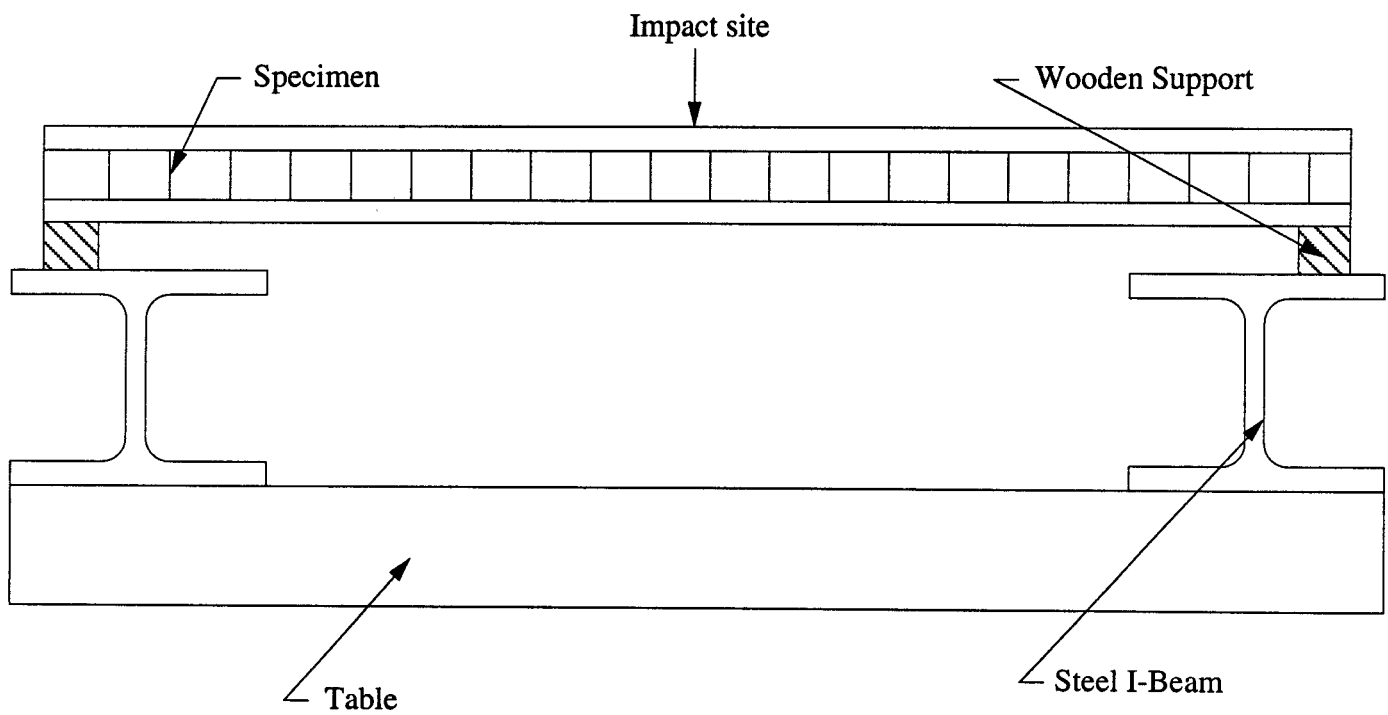


Figure 7. Strain gage layout for notched specimens 8, 9, and 10. Dimensions are in inches. Viewed from the specimen concave surface. Bold lines indicate back-to-back strain gage pairs, all other gages are mounted on the specimen concave surface.



Front View



Side view

Figure 8. Specimen setup used to impact the specimens.



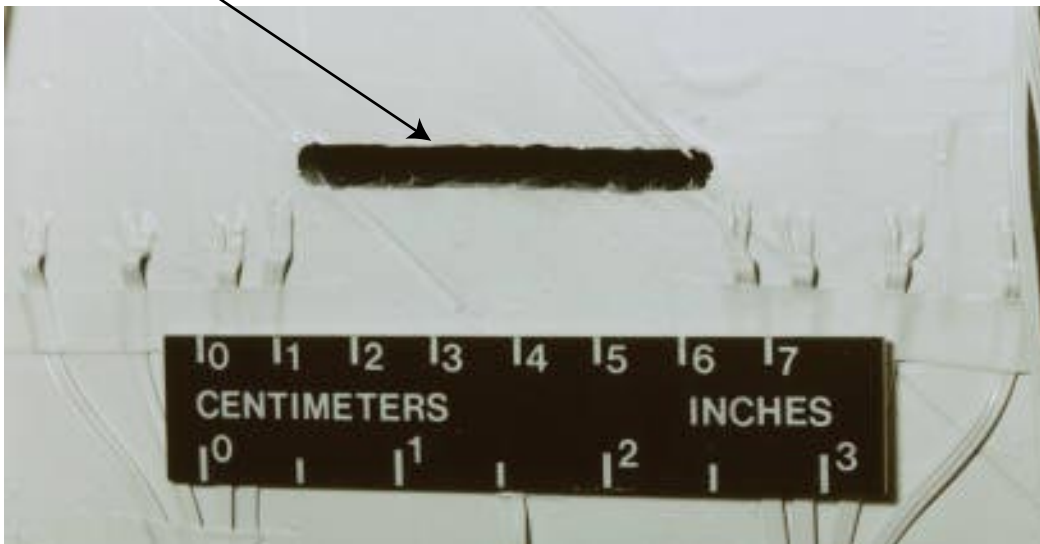
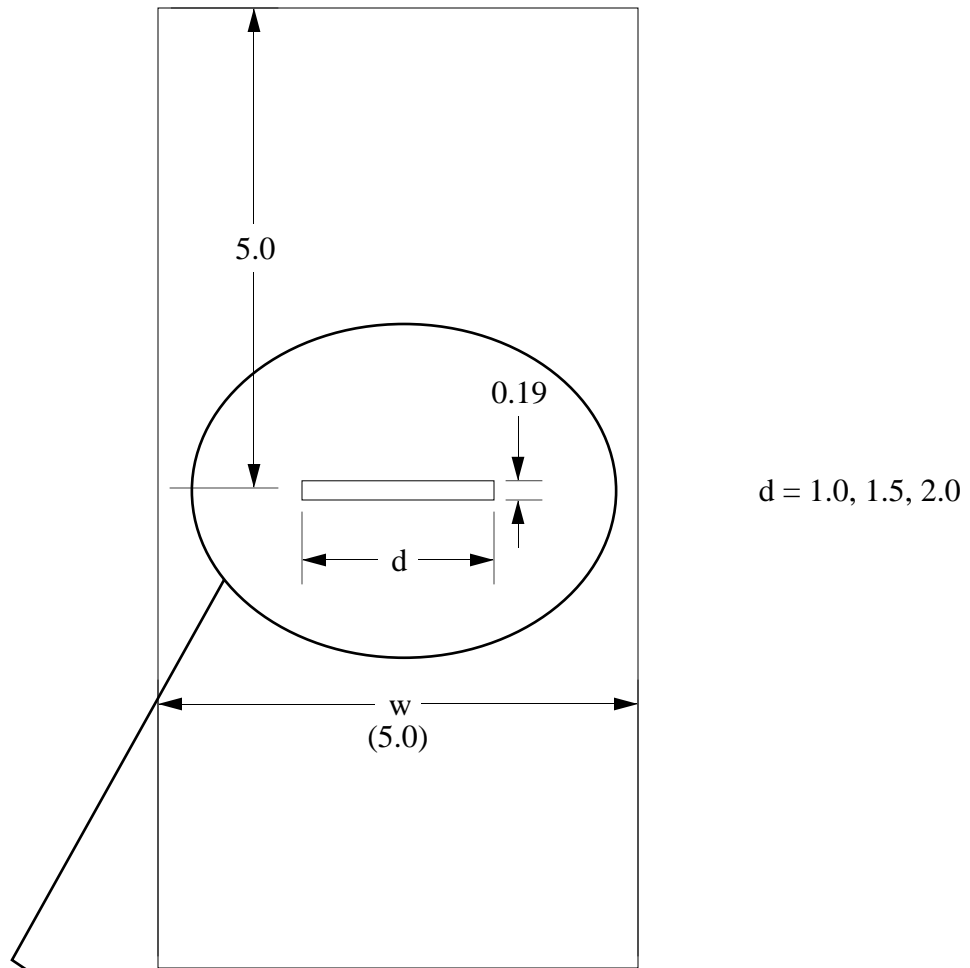
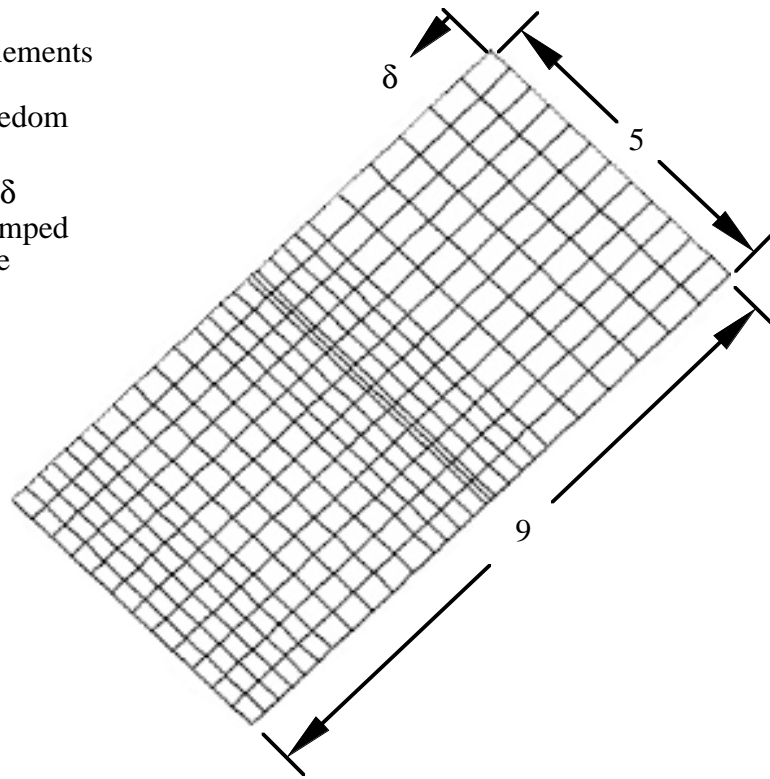


Figure 9. Details of machined notch. Dimensions are in inches.

324 modified thick-shell elements

5,080 active degrees of freedom

- Uniform end shortening,  $\delta$
- Five-inch-wide edges clamped
- Nine-inch-long edges free

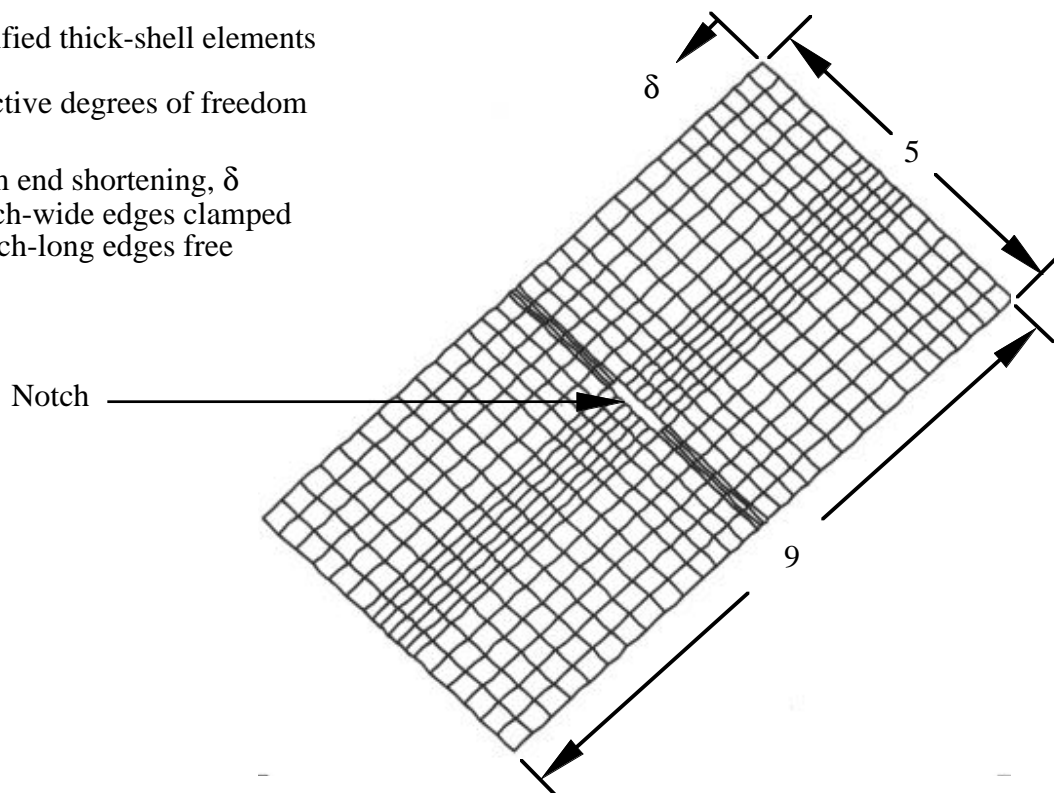


(a) Model of undamaged specimen

702 modified thick-shell elements

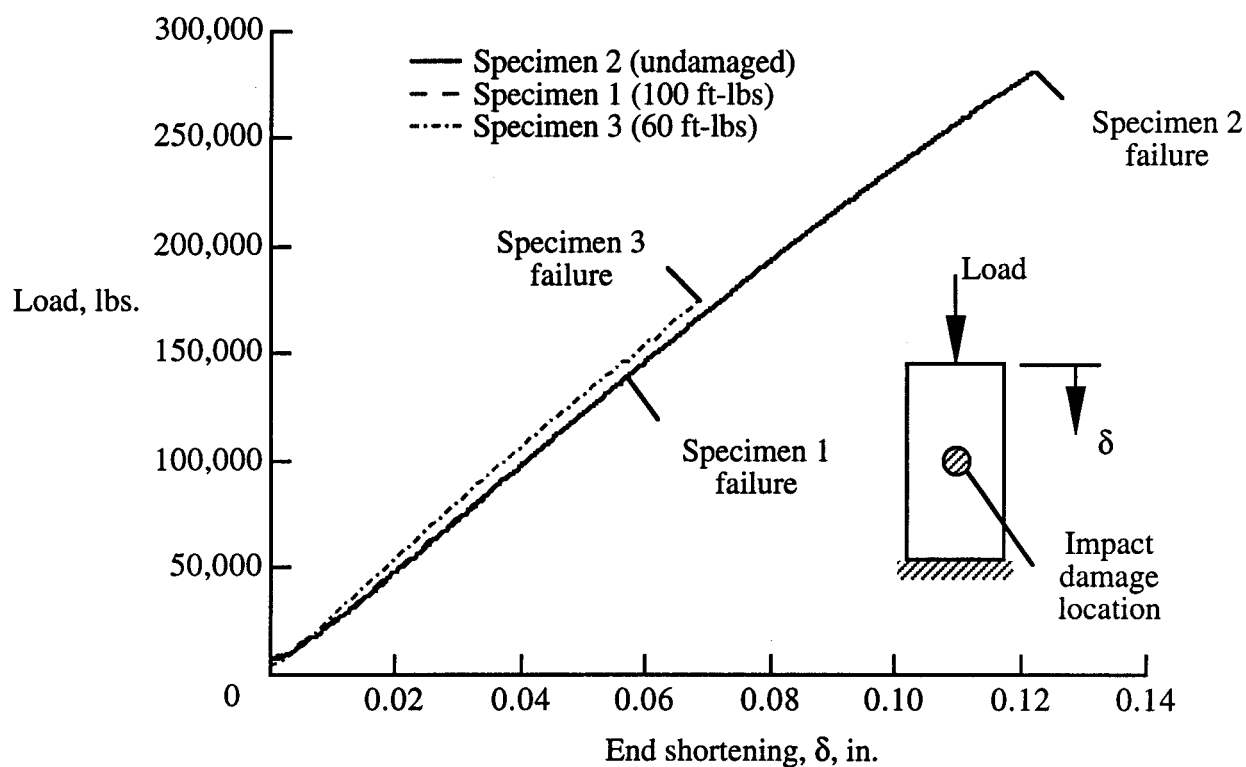
10,941 active degrees of freedom

- Uniform end shortening,  $\delta$
- Five-inch-wide edges clamped
- Nine-inch-long edges free

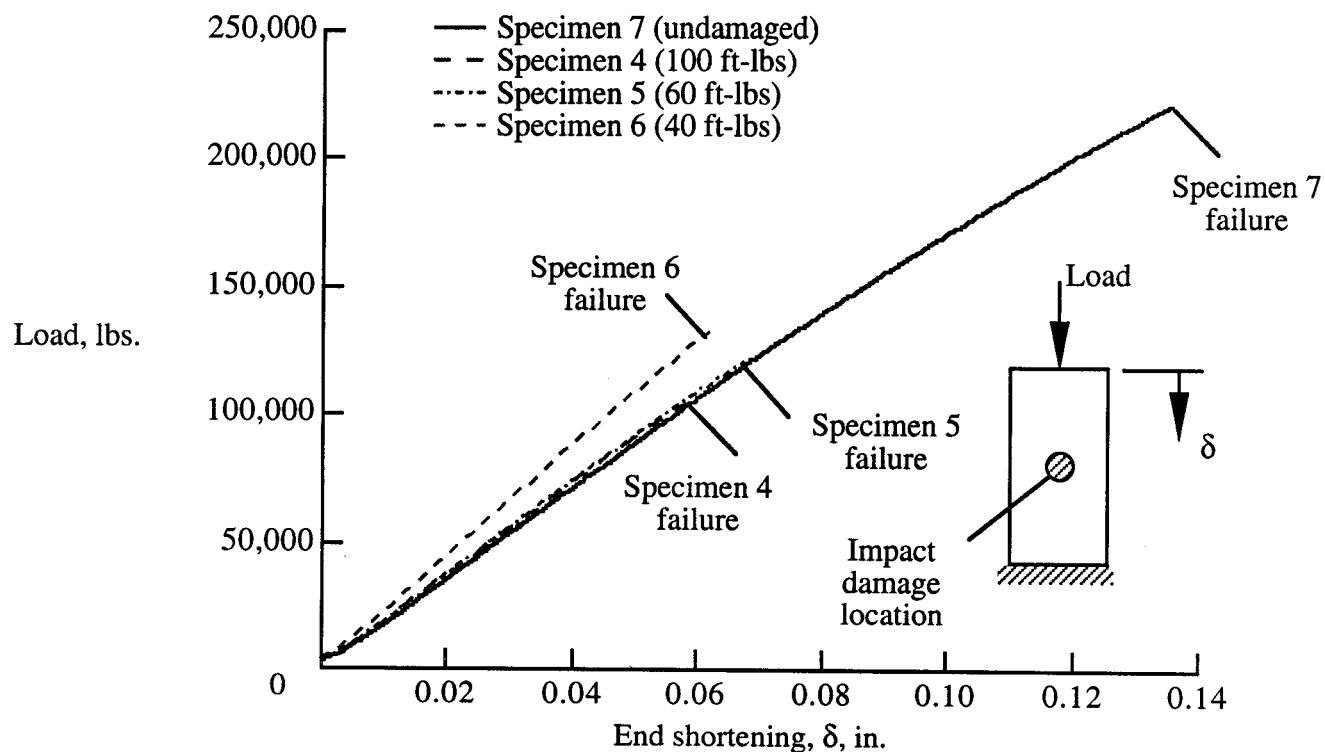


(b) Model of notched specimen

Figure 10. Finite element models of undamaged and notched specimens.  
Dimensions are in inches

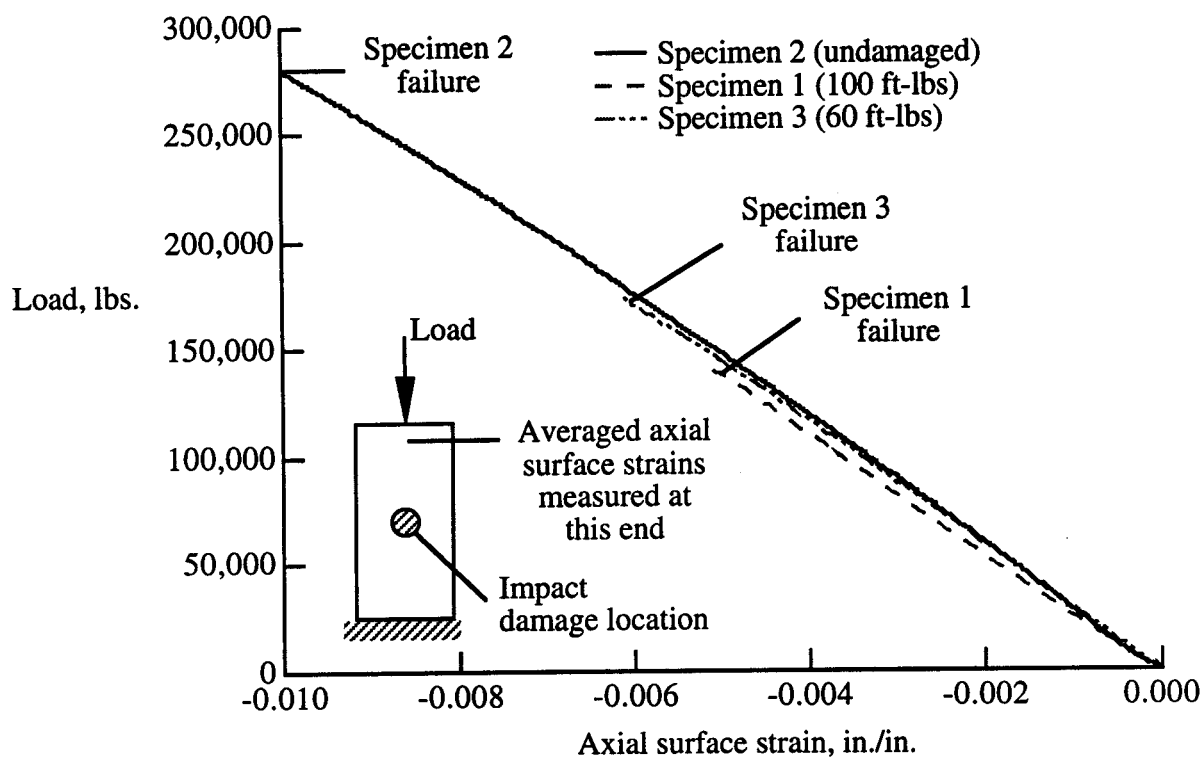


(a) Specimens 1 - 3

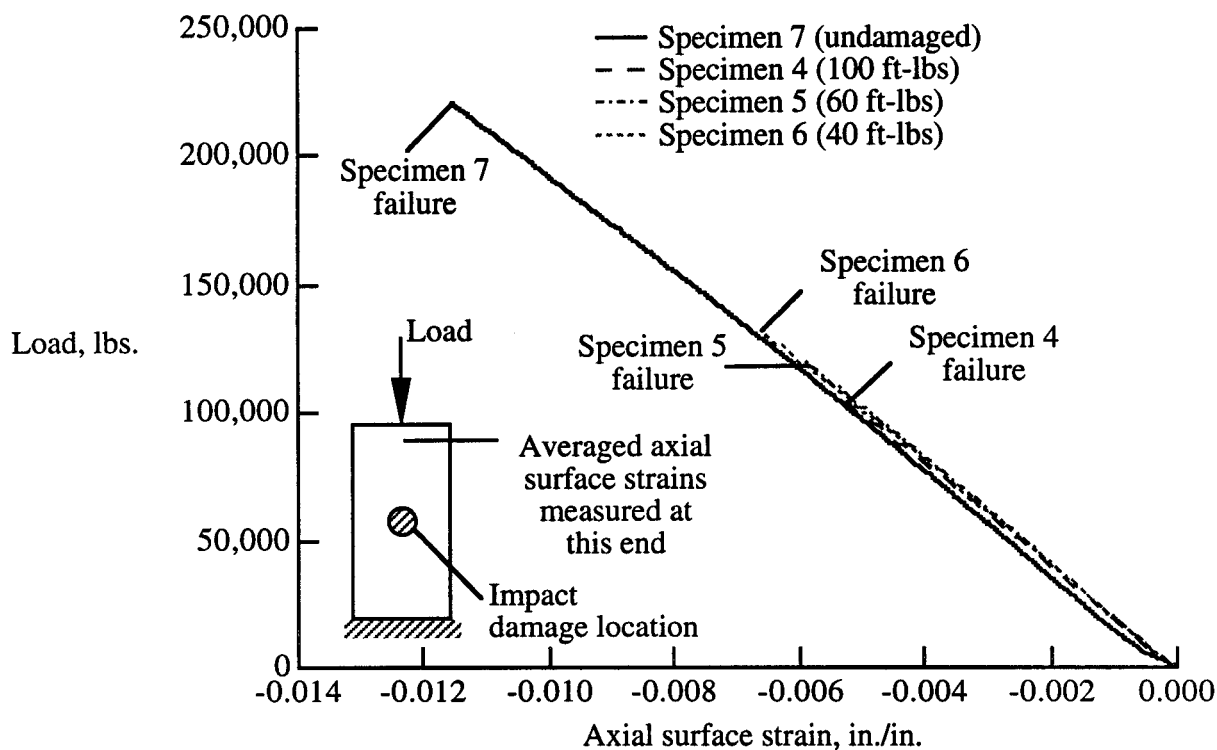


(b) Specimens 4 - 7

Figure 11. Experimental load-shortening results for the CAI study.

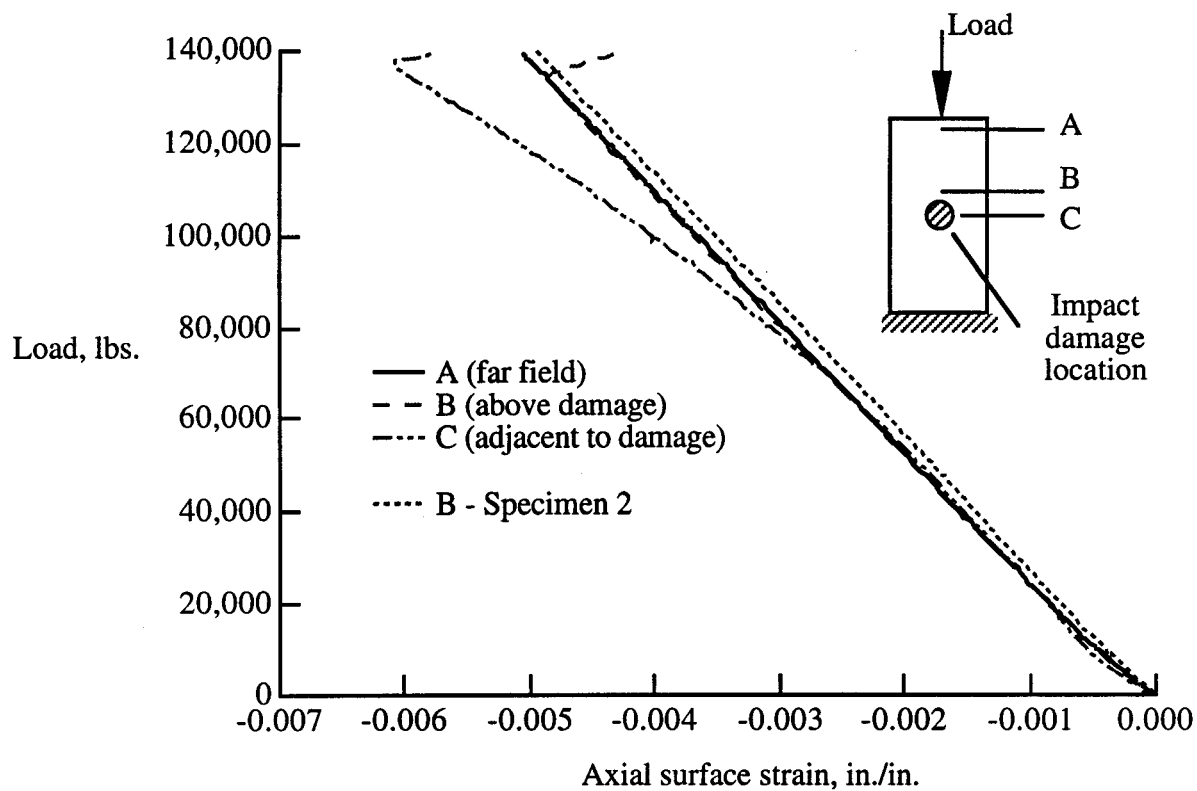


(a) Specimens 1 - 3

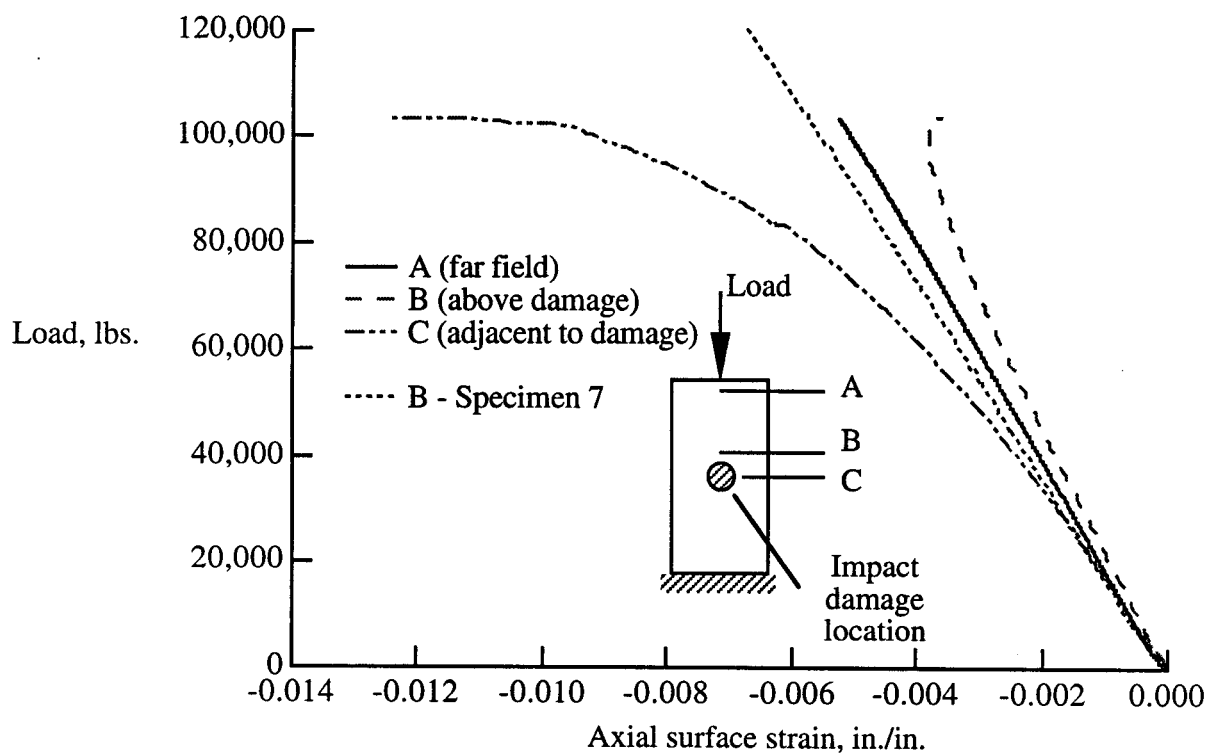


(b) Specimens 4 - 7

Figure 12. Experimental axial surface strain results for the CAI study.



(a) specimen 1 (100 ft-lbs of impact energy)



(b) Specimen 4 (100 ft-lbs of impact energy)

Figure 13. Experimental axial surface strain results from the CAI study.

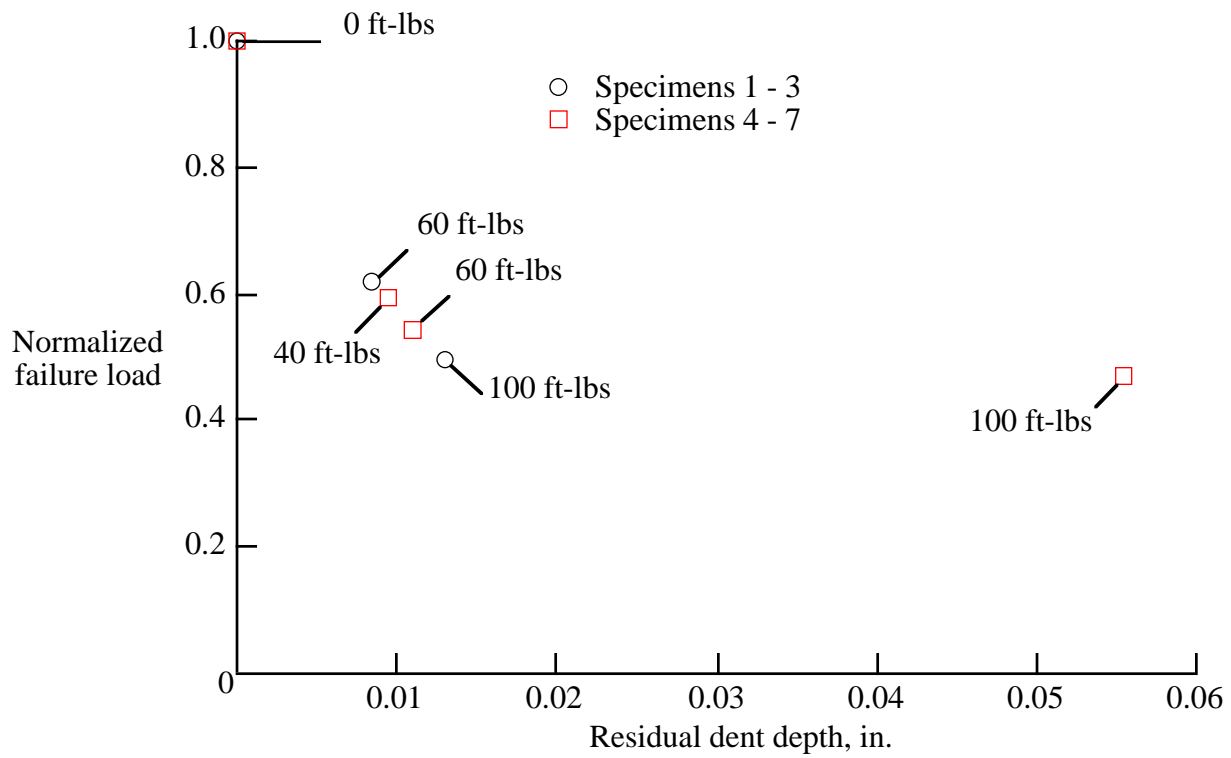


Figure 14. Normalized failure loads as a function of residual dent depth for the CAI specimens. CAI failure loads normalized with respect to undamaged specimen failure loads.

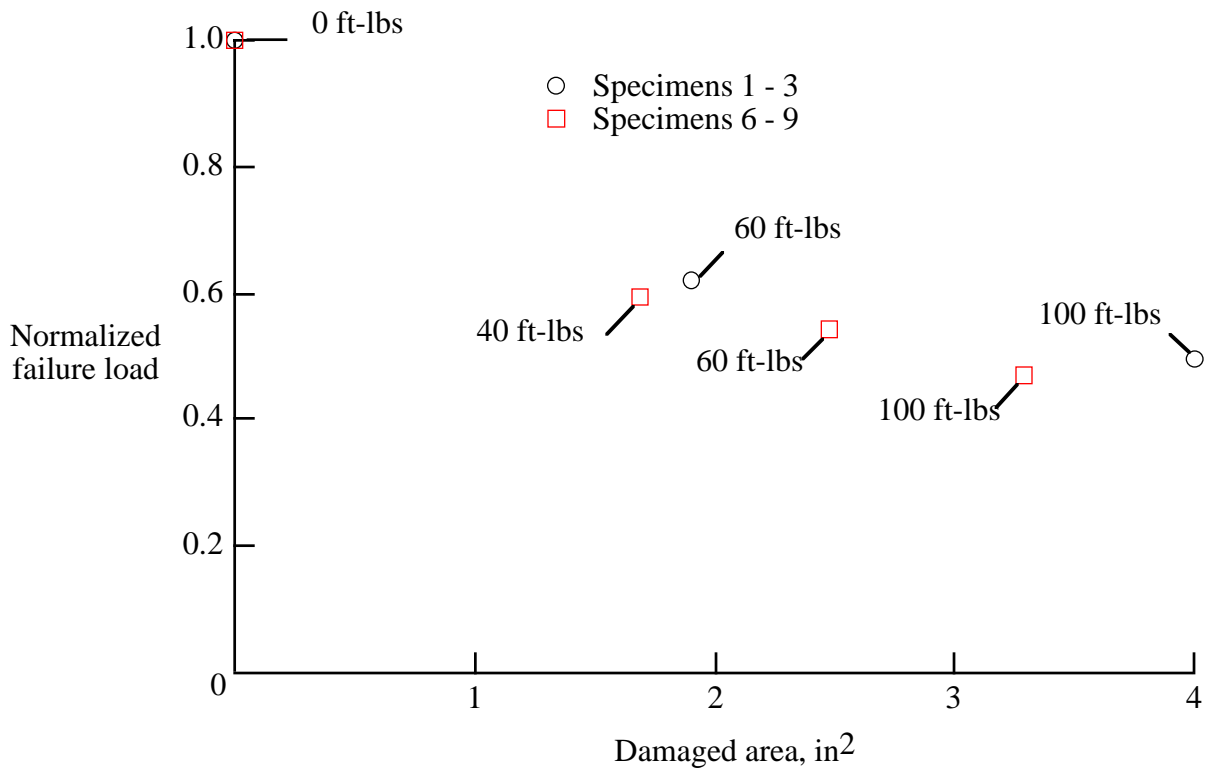


Figure 15. Normalized failure loads as a function of damaged area for the CAI specimens. CAI failure loads normalized with respect to undamaged specimen failure loads.

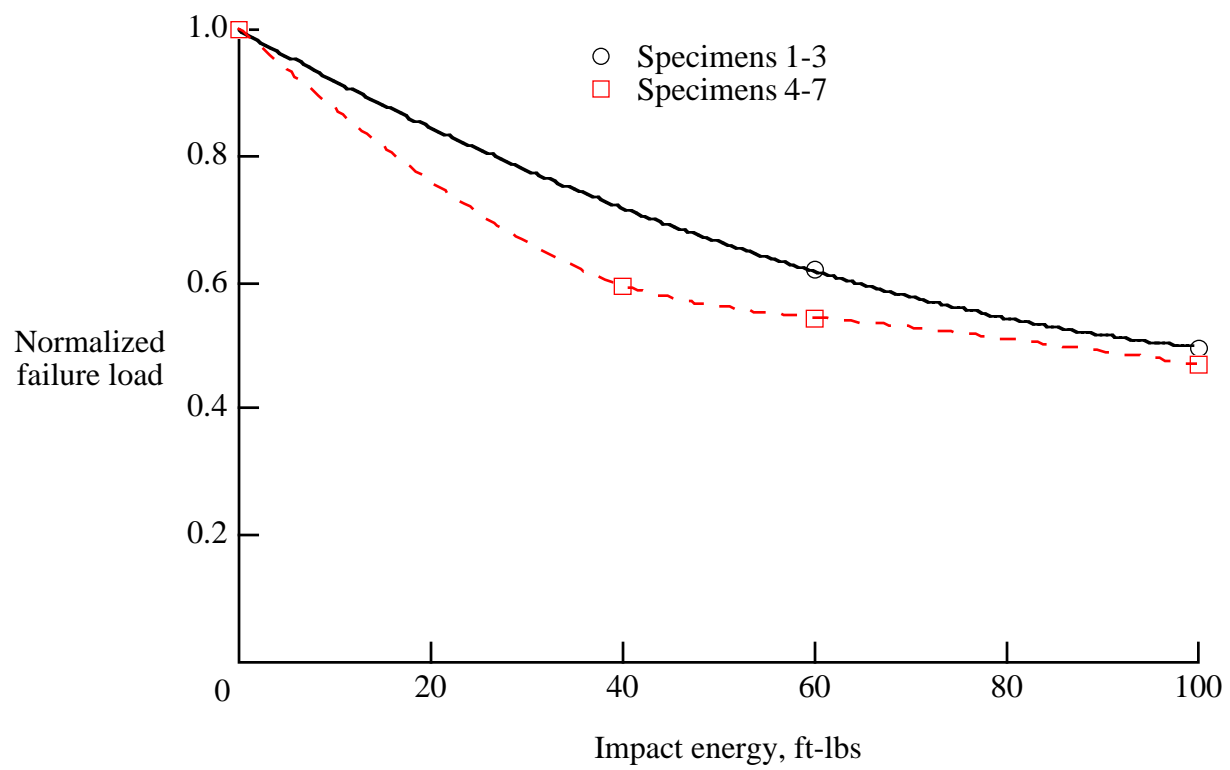
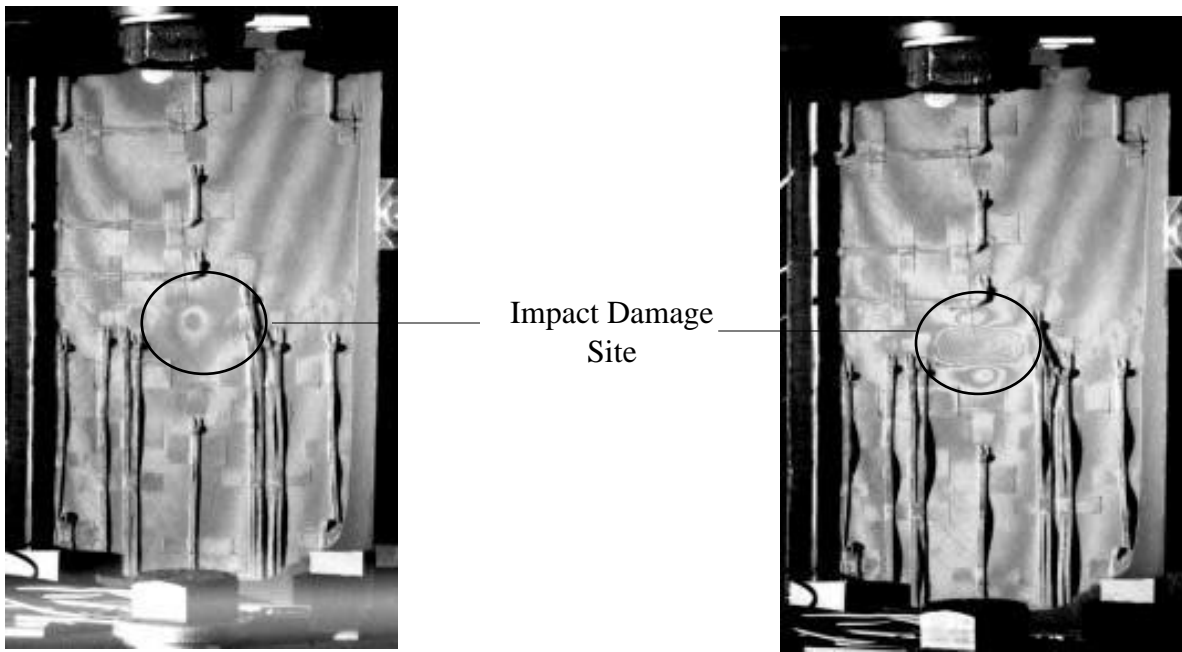


Figure 16. Normalized failure loads as a function of impact energy for the CAI specimens. CAI failure loads normalized with respect to undamaged specimen failure loads.



(a) Applied load = 0 lbs

(b) Applied load = 130 kips

Figure 17. Moiré fringe patterns for CAI specimen 8 (40 ft-lbs of impact energy).

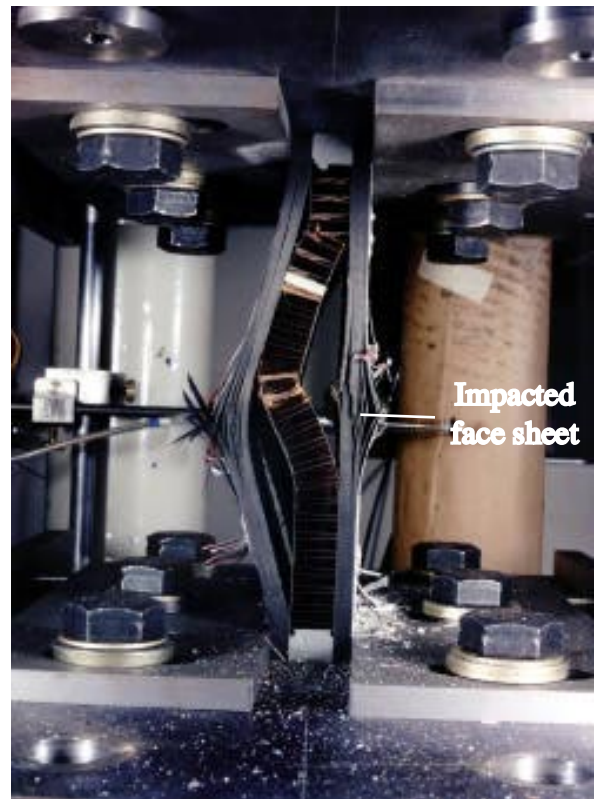
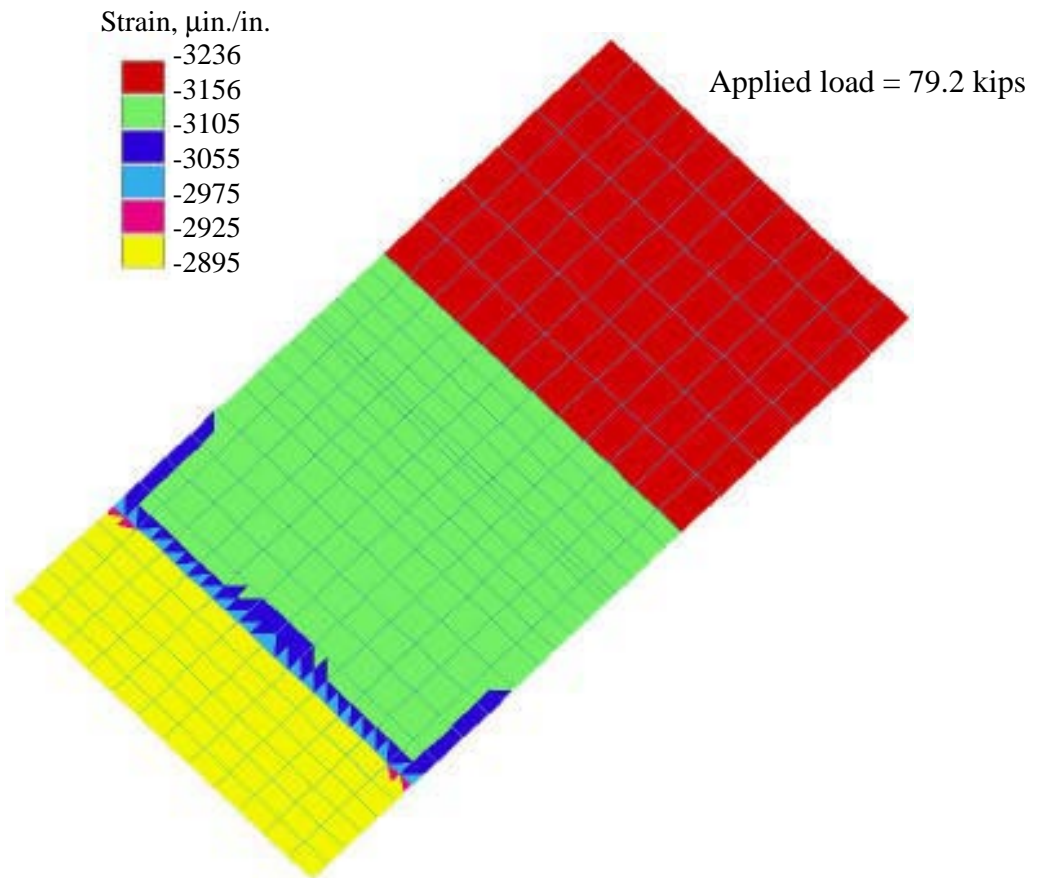
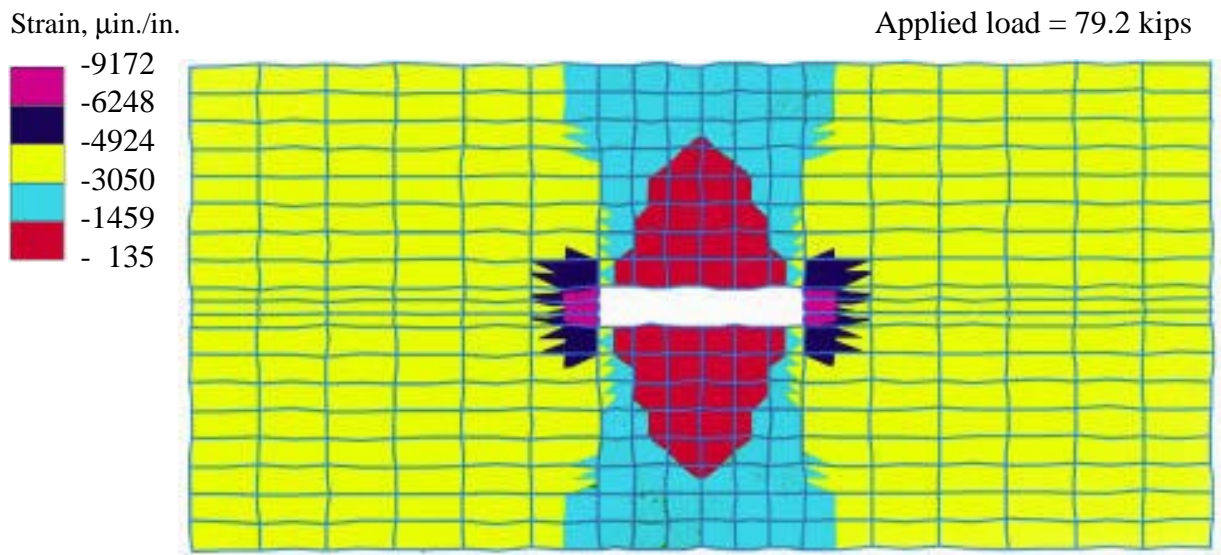


Figure 18. Failure mode for CAI specimen 3 (failure load = 173.5 kips).





(a) Unnotched specimen 10



Expanded view of notched region

(b) Notched specimen 10 (1.0-in.-long notch)

Figure 19. Analytical surface strain contours for specimen 10 without and with a 1.0-in-long notch.

Applied load = 80.0 kips



(a) Experimental strain contours

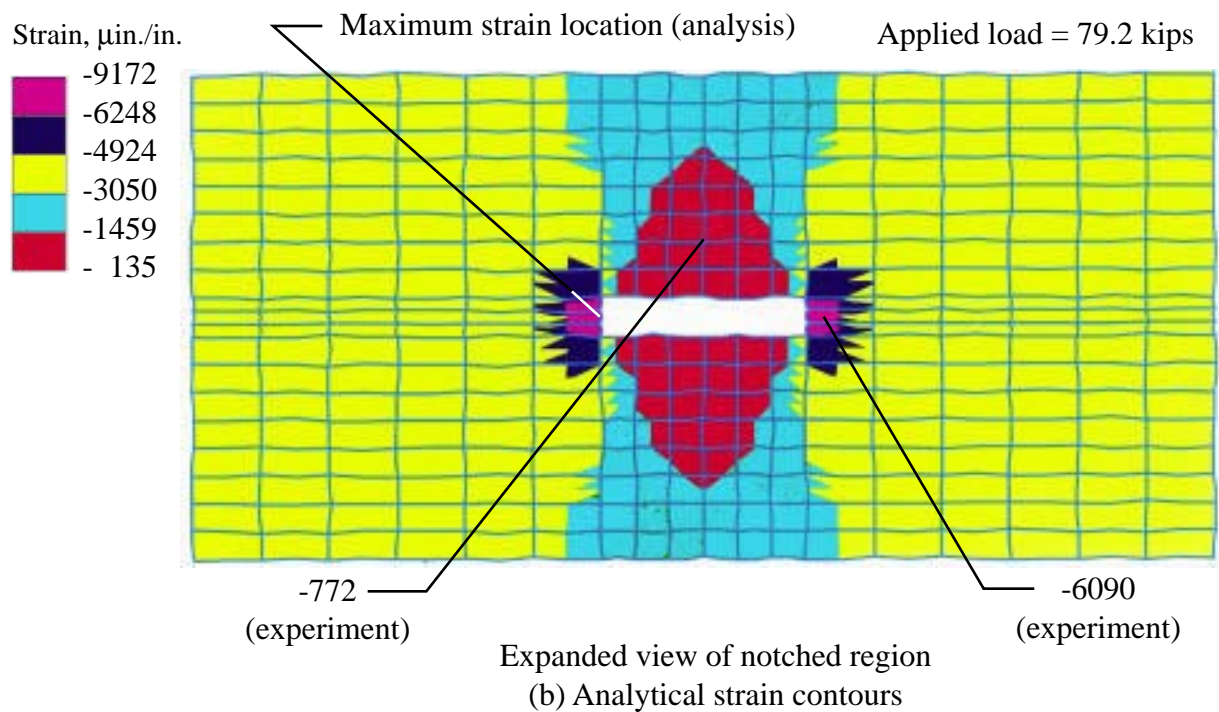


Figure 20. Experimental and analytical strain contours for specimen 10 (1.0-in.-long notch). Strains are in  $\mu\text{in./in.}$

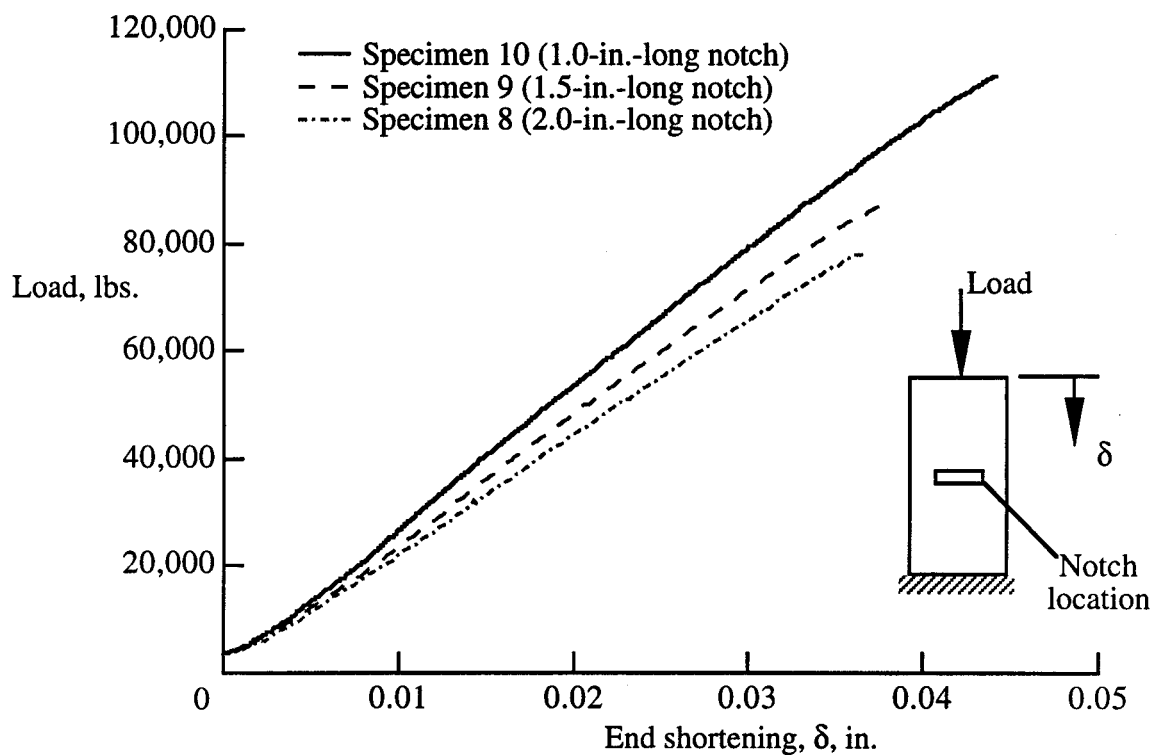


Figure 21. Experimental load-shortening results for the notched specimens (8 - 10).

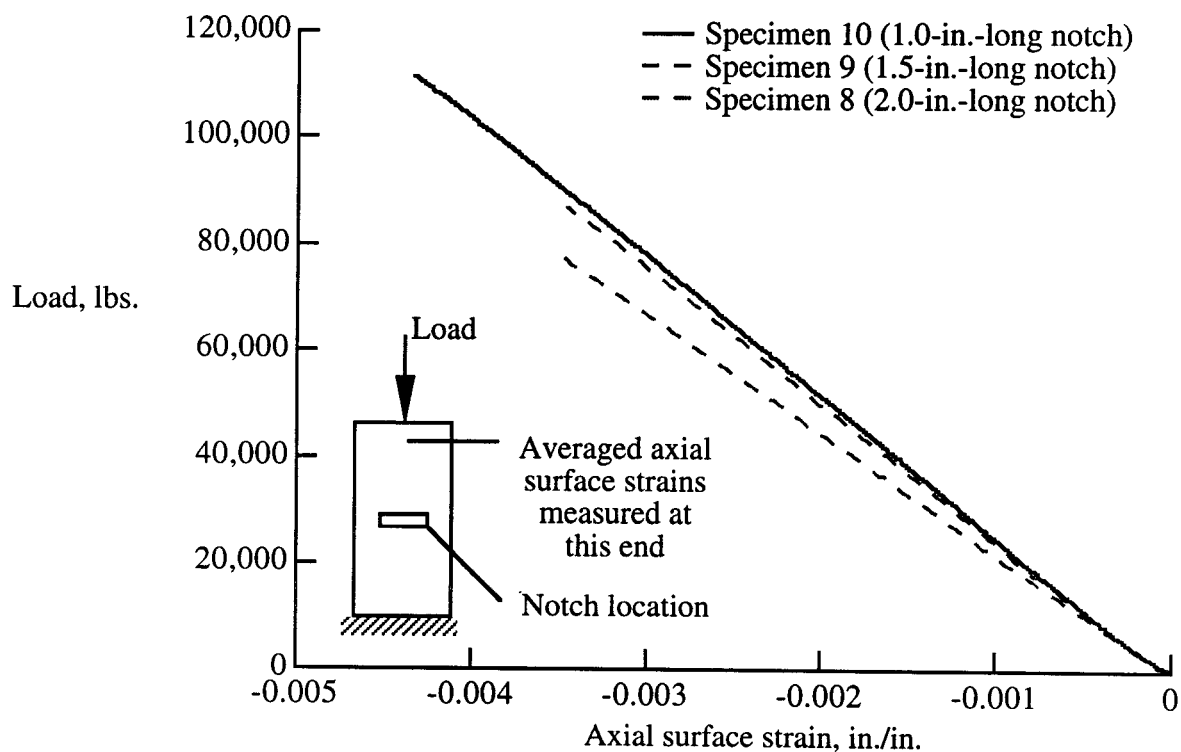
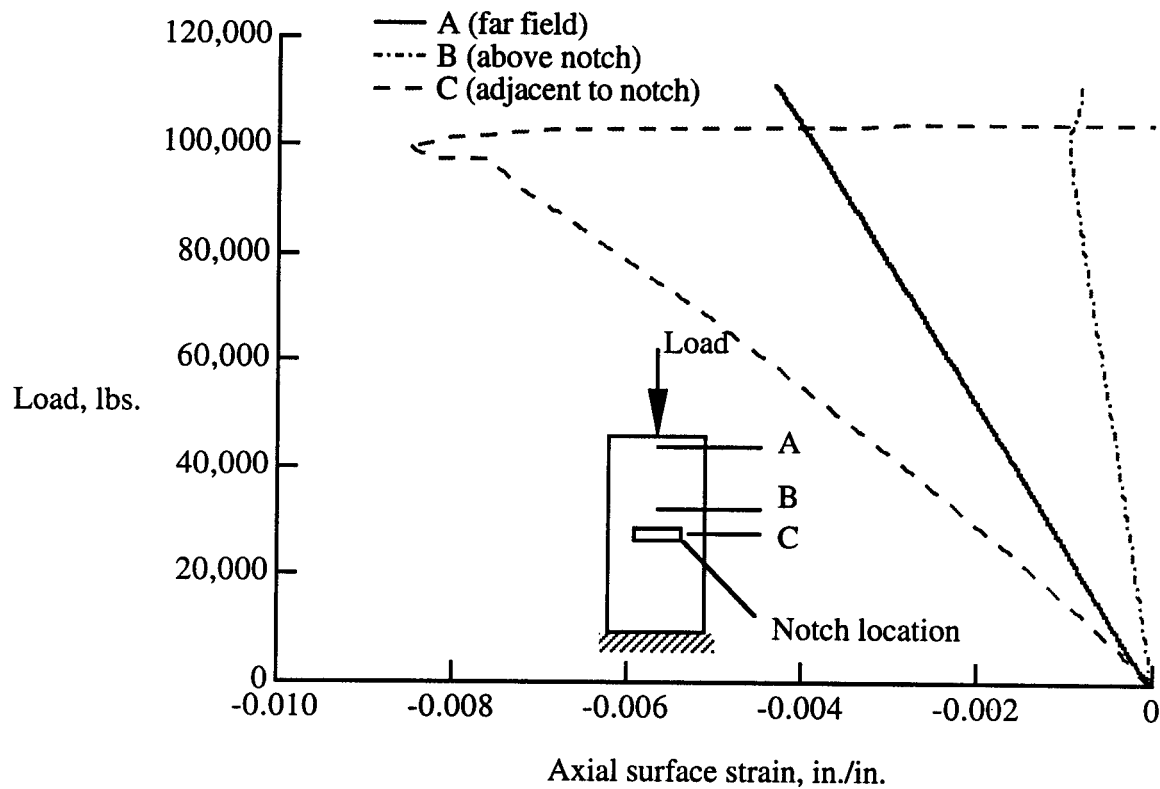
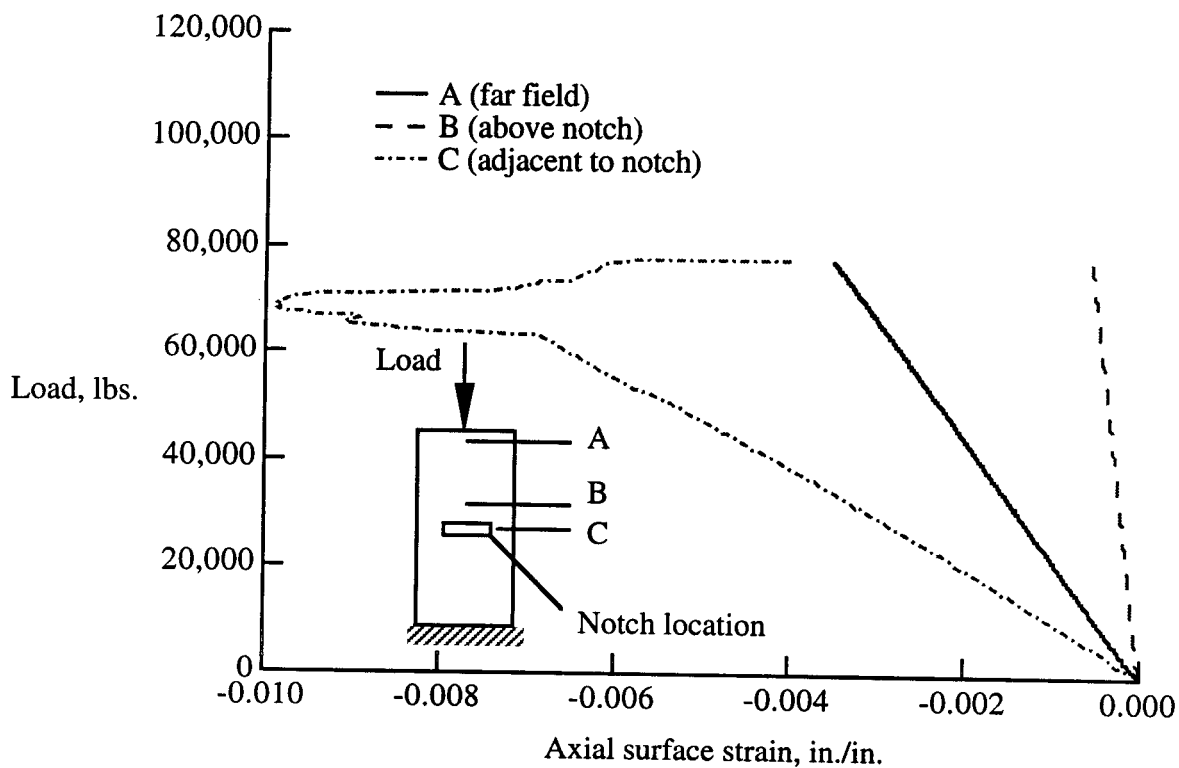


Figure 22. Experimental axial surface strain results for the notched specimens (8 - 10).



(a) Notched specimen 10 (1.0-in.-long notch).



(b) Notched specimen 8 (2.0-in.-long notch)

Figure 23. Experimental surface strain results for notched specimens 8 and 10.

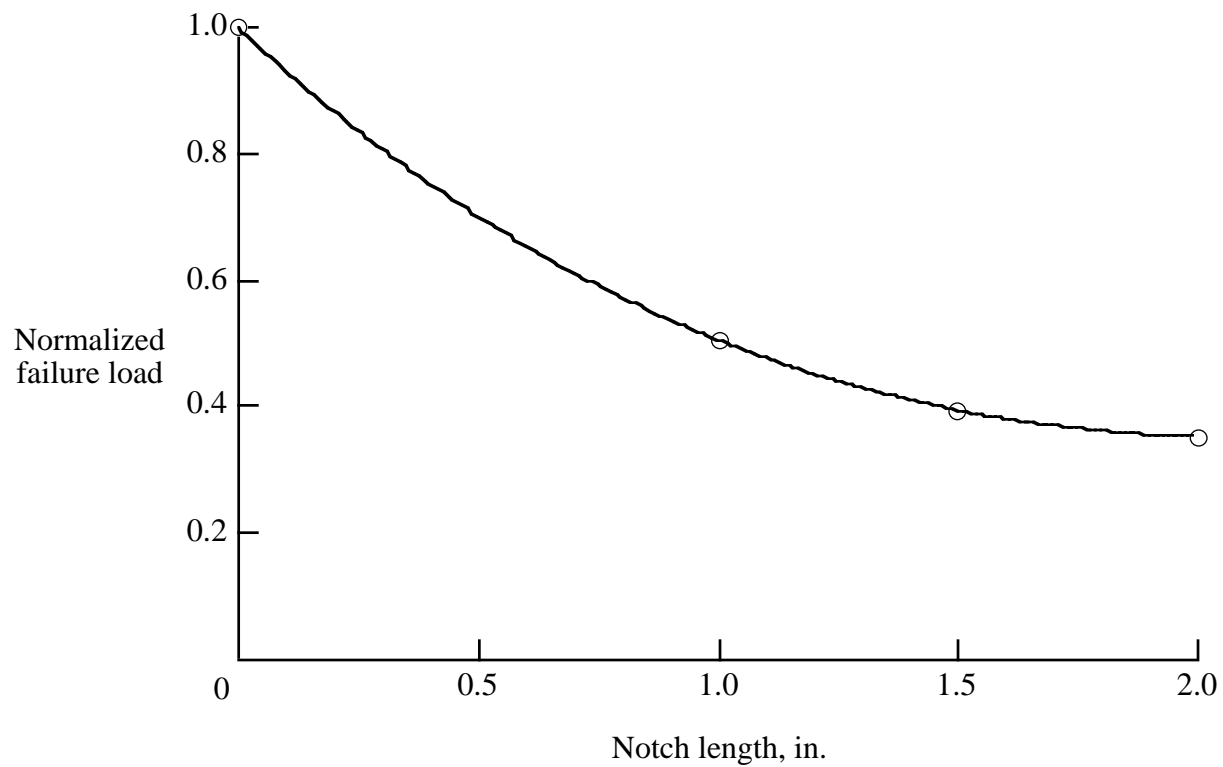


Figure 24. Normalized failure loads as a function of notch length for the notched specimens. Notched specimen failure loads are normalized with respect to the failure load for unnotched specimen 7.

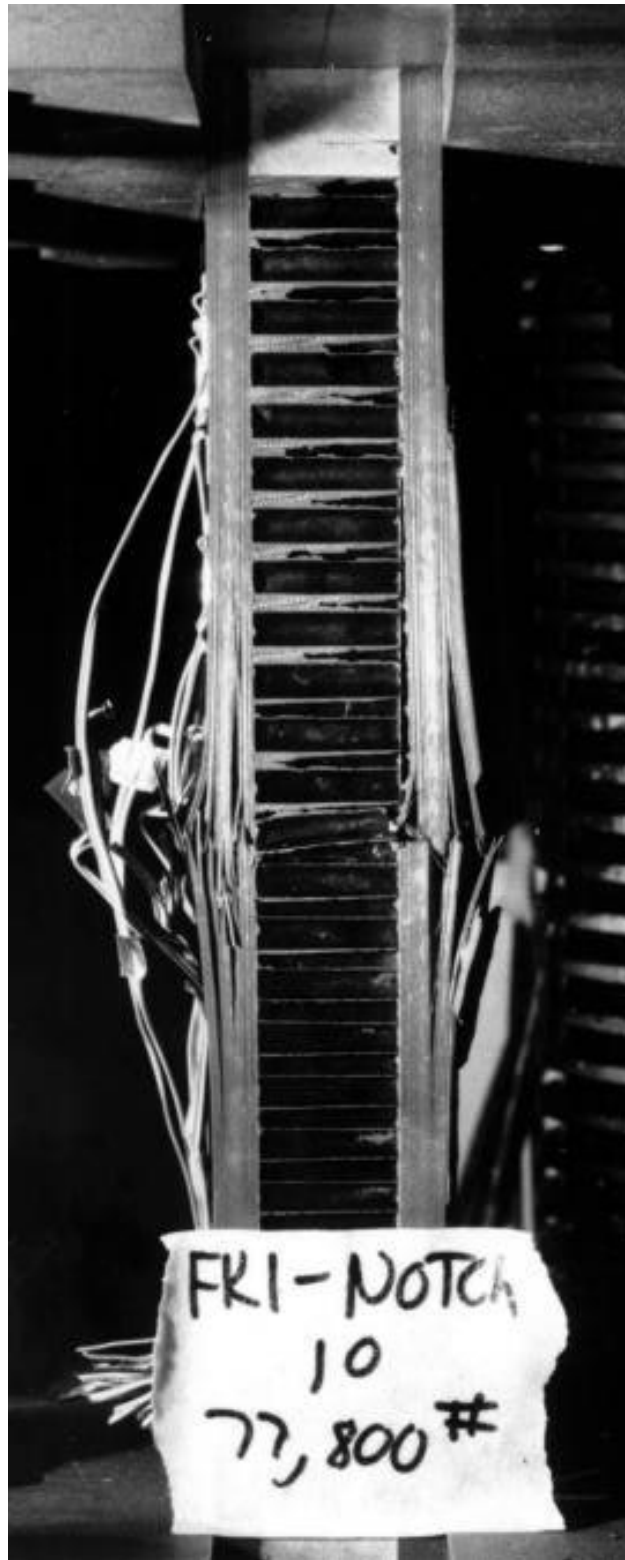


Figure 25. Failure mode for notched specimen 10 with a 2.0-in.-long notch (failure load = 77.8 kips).